Original Research

Hsp90 Inhibitor STA9090 induced VPS35 related extracellular vesicle release and metastasis in hepatocellular carcinoma

Wenchong Tan [a,1], Jinxin Zhang [a,1], Lixia Liu [a,1], Manfeng Liang [a], Jieyou Li [a], Zihao Deng [a], Zhenming Zheng [a], Yaotang Deng [a], Chenyang Liu [a], Yan Li [a], Guantai Xie [a], Jiajie Zhang [b], Fei Zou [a,*], Xuemei Chen [a,2,*]

[a] Department of Occupational Health and Medicine, Guangdong Provincial Key Laboratory of Tropical Disease Research, School of Public Health, Southern Medical University, Guangzhou, China
[b] Guangdong Provincial Key Laboratory of New Drug Screening, School of Pharmaceutical Sciences, Southern Medical University, Guangzhou, China

ABSTRACT

Heat shock protein 90 (Hsp90) has been an important therapeutic target for cancer therapy for decades. Unexpectedly, the monotherapy of N-terminal Hsp90 inhibitor STA9090 related clinical trials halted in phase III, and metastases were reported in animal models with the treatment of N-terminal Hsp90 inhibitors. Vacuolar protein sorting-associated protein 35 (VPS35) plays a vital role in endosome-derived EV (extracellular vesicle) traffic in neurodegeneration diseases, but no vps35 related EV were reported in tumors till now. Since tumor derived EVs contributes to metastasis and VPS35 is recently found to be involved in the invasion and metastasis of hepatocellular carcinoma (HCC), whether N-terminal Hsp90 inhibitor STA9090 induced EVs generation and the role of VPS35 in it were explored in this study. We found that N-terminal Hsp90 inhibitor STA9090 upregulated Bclaf1 and VPS35 levels, increased the secretion of EVs, and STA9090-induced-EVs promoted the invasion of HepG2 cells. As the clinical data suggested that the increased Bclaf1 and VPS35 levels correlated with increased metastasis and poorer prognosis in HCC, we focused on the Bclaf1-VPS35-EVs axis to further explore the mechanism of VPS35-related metastasis. The results demonstrated that Bclaf1 facilitated the transcription of VPS35 via bZIP domain, and knockdown of Bclaf1 or VPS35 alleviated pro-metastatic capability of STA9090-induced-EVs. All the results revealed the role of Bclaf1-VPS35-EVs axis on metastasis of HCC, and VPS35 knockdown decreased Hsp90 Inhibitor STA9090 induced extracellular vesicle release and metastasis, which provided a new combination therapeutic strategy to inhibit the metastasis of HCC caused by N-terminal Hsp90 inhibitor induced extracellular vesicles.

Introduction

HCC, the most common form of primary liver cancer [1], is the third leading cause of tumor-related death worldwide and accounts for the sixth cause of cancer incidence globally [2]. Because of the metastasis-associated poor prognosis and recurrence [3], HCC poses a major threat to human health, especially for patients in the advanced stage. Treatment failure is often with metastasis for cancer patients [4, 5], and accumulating evidence had shown that EVs played a prominent role in supporting cancer metastasis [6]. It had been reported that the traditional chemotherapy treatment of taxanes and anthracyclines could elicit tumor derived EVs to enhance the pro-metastatic capacity of breast cancer [7]. Therefore, further study on the inhibition of EVs-related invasion and metastasis is the key to improving the survival rate of HCC patients [8].

VPS35, as the core component of the conservatively heterotrimeric protein complex retromer [9], mediates endosomal cargo sorting into membrane tubules and buds [10]. Though the role of retromer in endosome-derived EV traffic is less clear, the evidence supports a role for the retromer in regulating excitatory synaptic transmission [11]. VPS35 mutation was originally found to be linked with Parkinson's Disease [12]. Accumulating evidence showed that retromer dysfunction could

cause neurodegeneration diseases like AD, ALS; Interestingly, VPS35 has recently been identified as a novel oncogene by a whole-exome and RNA sequencing in a small HCC cohort [13]. VPS35 can exert its oncogenic roles to promote tumor growth, invasion, and metastasis through the PI3K-AKT, Wnt/non-canonical planar cell polarity (PCP) signaling pathway, and KLF7/VPS35 axis [14,15]. Nevertheless, the in-depth regulation mechanism of VPS35 in EVs related HCC invasion and metastasis remains unknown till now.

The 90-kDa Heat shock protein (Hsp90) is the most abundant chaperone in cells [16], and more than 200 Hsp90 client proteins are important in signaling pathways and drive tumor cell progression and metastasis [17]. For more than 2 decades, Hsp90 has been the hot therapeutic target for cancers. Structurally, Hsp90 comprises three conserved domains: N-terminal domain (NTD), middle domain (MD), and C-terminal domain (CTD) [17]. Ganetespib (STA9090), as an N-terminal Hsp90 inhibitor, competitively binds to the Hsp90 ATP binding site to abrogate the ATPase activity and presents potent anticancer activity in a variety of solid tumors. Though Ganetespib (STA9090) is the only Hsp90 inhibitor that entered phase III of clinical trials [18], the monotherapy of N-terminal Hsp90 inhibitor Ganetespib (STA9090) related clinical trials halted in phase III and metastases were reported in animal models with the treatments of N-terminal Hsp90 inhibitors [19]. Hence, the mechanism of N-terminal Hsp90 inhibitor-related pro-metastatic effects is urged to be further explored, then the precise combination therapy with N-terminal Hsp90 inhibitors can be found.

One of the important differences between N-terminal and C-terminal inhibitors of Hsp90 is the effects on HSF1 (Heat shock factor 1) activation. HSF1 mainly exists in the cytoplasmic with the form of monomer, and in the stress-free condition, Hsp90 inhibits the transcriptional activity of HSF1 via the Hsp90-HSF1 complex, and HSF1 activation [20] can be triggered by N terminal Hsp90 inhibitor. Unfortunately, HSF1 activation promotes the growth of malignant cells in several tumors type and correlates with poor prognosis [21–23].

The other important difference between N-terminal and C-terminal inhibitors of Hsp90 is the effects on Bcl-2 associated transcription factor 1 (Bclaf1), as we reported [24]. Novobiocin (NB) is a C-terminal Hsp90 inhibitor, the CTD inhibitor disrupts the interaction between co-chaperone and client proteins. NB treatment decreased the protein level of Bclaf1 and the protein stability of Bclaf1 is dependent on the C-terminal of Hsp90 [24]. Bclaf1 was initially identified as an interaction partner with E1B, an anti-apoptotic Bcl-2-related protein, which was reported to participate in the regulation of cell apoptosis [25]. Growing evidence has shown that Bclaf1 has a much broader function and involves in various biological processes, including not only pre-mRNA splicing and mRNA processing, DNA damage and repair, but also gene transcription [24,26]. The Bclaf1 protein contains the basic zipper (bZIP) and Myb DNA-binding domain, which plays an important role in transcription regulation [27]. Recently, several studies had demonstrated that Bclaf1 played a pivotal role in promoting the proliferation, migration and invasion of cancer cells.

Hence, in this study, we focus on the effect of N-terminal Hsp90 inhibitor STA9090 on VPS35 related EVs formation, HCC invasion and metastasis and the transcriptional regulation mechanism of VPS35 affected by Bclaf1 in STA9090 treatment.

Materials and methods

Cell culture and reagents

Human hepatoma cell lines HepG2 (SCSP-510), Huh7 (SCSP-526), and normal liver cell line L02 (GNHu6) were purchased from the Chinese Academy of Sciences (Shanghai, China). MHCC97H cells were purchased from Liver Cancer Institute, Zhongshan Hospital, Fudan University (Shanghai, China). MHCC97H-RFP cell line was a kind gift from School of Laboratory Medicine and Biotechnology, Southern

Medical University (Guangzhou, China). All cell lines were confirmed free from *Mycoplasma* pollution with MycAwayTM-Color One-Step Mycoplasma Detection Kit (Yeasen, Shanghai, China). The above cell lines were incubated in Dulbecco's modified Eagle's medium (DMEM, Gibco, USA) with 10% fetal bovine serum (FBS, Gibco, USA) and 1% streptomycin and penicillin at 5% CO_2, 37°C. Hsp90 inhibitors Ganetespib (STA9090, S1159) and Novobiocin (NB, S2492) were purchased from SelleckChem (Houston, TX, USA).

Human tissue sample collection

This patient's study was approved by the ethical committee of NanFang Hospital (Guangzhou, China) (Approval Code: NFEC-2022–184), all patients provided written informed consent for the use of surgical samples. Fresh HCC tissue and adjacent nontumoral tissue samples were collected from 11 patients who were diagnosed with HCC in NanFang Hospital (Guangzhou, China) during surgery. None of the patients had been treated with radiotherapy or chemotherapy before performing the hepatectomy.

Cell viability assay

The cell viability of EVs was measured by a Cell Counting Kit-8 (CCK-8) assay (Dojindo, #CK04, Tabaru, Mashikimachi, Japan). HepG2 cells were seeded into 96-well plates at the density of 5×10^3 cells per well and treated with STA9090 or NB or co-cultured with 0.2 µg of siNC-EVs/siNC-STA9090-EVs/siVPS35-EVs/siVPS35-STA9090-EVs, then incubated for 24 h at 37°C and 5% CO_2. The absorbance of all groups was quantified at 450 nm via a microplate reader (Thermo, MK3). All the experiments were performed in triplicate times.

Cell cycle assay

1×10^6 HepG2 cells were seeded in the six-well plates with 10% FBS DMEM. Cells were treated with Hsp90 inhibitors (STA9090/NB) or co-cultured with 10 µg of EVs (C/STA9090/NB-induced) for 24 h (5% CO_2, 37 °C). Then cells were harvested and immediately fixed with 75% ethanol at −20 °C (overnight). For the cell cycle analysis, cells were stained with PI (50 µg/mL, RN3501, Aidlab Biotechnologies Co Ltd, Beijing, China) and RNase (50 µg/mL, R30396–10×1 ml, YuanYe Bio-Technology Co Ltd, Shanghai, China) for 30 min separately, and cell cycle was detected by Guava easyCyte Flow Cytometry System (6HT2L, Millipore, MA, USA). The data were analyzed by the Modfit software 4.2 (BD Biosciences, Franklin Lake, New Jersey, USA).

Cell transfection

Cell transfection was performed with Lipofectamine 3000 transfection reagent (L3000015, Life Technologies, USA) according to the instruction. The siBclaf1 and siVPS35 sequences were synthesized by Synbio Technologies (Suzhou, China). The empty vector (EV), Bcalf1 full-length plasmid (FL) and ΔMyb Bclaf1 plasmids were kindly provided by Dr. Tang (College of Veterinary Medicine, China Agricultural University). And we designed a vector expressing FLAG fusion constructs encoding a bZIP domain (112–130aa) deleted Bclaf1 mutant (ΔbZIP). The siRNA sequences were listed in Supplementary Table 1.

Lentiviral transfection

HepG2 cells (1×10^5 cells) were seeded into the 6-well-plate and cultured for 12 h. On the next day, shNC-GFP or shVPS35-GFP or shBclaf1-GFP lentivirus was added to each well at the most suitable MOI, mixing it before continued incubating for 24 h. Then, cells were collected and incubated in selection medium containing 1000 µg/mL G418 (shNC/shVPS35) or 1 mg/mL puromycin (shBclaf1) for 2 weeks. The protein expression of VPS35 and Bclaf1 was detected by western

blotting.

Exosomal-free FBS medium preparation

The FBS was dispensed into the ultracentrifuge tubes and balanced with an electronic scale. Then the FBS has subjected to 16 h (overnight) ultracentrifugation at 120,000 g (TYPE 70.1Ti rotor, Beckman, USA) at 4 °C. After that, the FBS was filtered with a 0.22 μm filter and stored at −20°C. The Exo-free medium consisted of 10% exosome-free FBS and 500 mL basic medium [28].

Isolation of EVs from culture medium [29]

The culture medium was subjected to serial centrifugation to respectively remove the cells and debris (500 g for 10 min) and cell debris and large vesicles (2000 g for 30 min). Mixed the medium with an equal volume of 16% PEG-enriched sedimentation solution (7.68 g PEG powder and 2.81 g NaCl were dissolved into the 48 mL sterile water) and shook slowly at 4 °C and incubated overnight. On the next day, the mixture was centrifuged at 3420 g for 1 h at 4 °C, discarded the supernatant, and resuspended the pellet with 13 mL PBS. Then the mixture was transferred to Ultra-Clear centrifuge tubes (#344,059, Beckman) and centrifuged at 100,000 g for 70 min at 4 °C using the SW-41Ti rotor in an Optima XPN-100 ultracentrifuge (Beckman, USA). Pelleted vesicles were suspended in 200 μL of PBS or 200 μL of strong Exosome-Lysis solution (5%SDS, 10 mM EDTA, 120 mM Tris–HCl pH6.8, 2.5% β-mercaptoethanol, 8 M Urea) by vortexing, followed by adding 50 μL 5 x loading buffer in it and transferred to a new 1.5 EP tubes. The BCA method was used to detect the EVs-protein concentration, which can use for WB or stored at −80 °C after aliquoting.

Transmission electron microscopy and nanoparticle tracking analysis

Transmission electron microscopy (TEM) was applied to identify the purified extracellular vesicles (EVs). Purified EVs from the culture medium were resuspended in PBS. Approximately 30 μL of EVs was dropped onto grids for 3 min, and then immediately stained with 30 μL 3% phosphotungstic acid (PH7.0) for 3 min and dried for 20 min. For each step, excess liquid was removed by wicking with filter paper. Grids were imaged using the JEM-1400 TEM (JEOL, Japan). All EVs images were collected at 6,000X and 25,000X with an advanced microscopy camera.

For size distribution of EVs, nanoparticle tracking analysis (NTA) was performed by a NanoSight NS300 (Malvern, UK) equipped with a 405 nm laser and a sCMOS camera. Resuspended EVs were diluted 100 or 300-fold in filtered PBS to achieve a final concentration of 10^8 particles/ml. The NTA 3.2 Dev Build 3.2.16 software (Malvern, UK) was used for data analysis.

Dynamic light scattering

The hydrodynamic diameter of EVs was analyzed by Zetasizer Nano-ZS90 (Malvern, UK) according to the manufacturer's instructions. The EVs samples were diluted to 1 mL PBS and resuspended. And the hydrodynamic diameters reported were the average of three separate measurements of a single sample.

Wound scratch assay

Cells were grown in 6-well plates until 90% confluence, then the wounds were scratched in each well straightly with a 200-μL pipette tip. Before culture in 1% FBS DMEM, the debris and shedding cells were removed by washing with PBS. The wound distance of cell migration at 0 h and 24 h were photographed by an Inverted digital imaging microscope (Eclipse TS100LED-F MV, Nikon, Japan) in 4 x objective lens. The migration areas of the wounds were analyzed by Image Pro-Plus 6.0.

Transwell assay

The ability of cell migration and invasion were assessed by transwell assay (Cell Culture Insert: PET Membrane 8 μm, pore size 6.5 mm diameter, #3422, Corning, USA). Cells were cultured in the 1% FBS DMEM for 24 h before seeding to the Cell Culture insert. For invasion assay, cells (5×10^4) resuspended in 200 μL of basic medium and 2 μg of EVs extracted from the culture medium (STA9090/NB treatment) were added into the upper chamber coating with Matrigel (1:5 dilution, #356,234, BioCoat, USA). Meanwhile, 10% FBS DMEM was added to the lower chamber. The chambers were incubated for 24 h (5% CO_2, 37 °C), then removed the remaining cells in the upper chamber with a cotton swab, fixed in 4% paraformaldehyde for 20 min, stained for 10 min with 0.1% crystal violet, and photographed 6 pictures randomly using an Inverted digital imaging microscope (Eclipse TS100LED-F MV, Nikon, Japan) in 10 X objective lens. The numbers of cells/field were analyzed by Image Pro-Plus 6.0. While for migration assay, the procedure was similar to the invasion assay without Matrigel coating.

Western blotting

Western blotting was performed as described previously [24]. The primary antibodies were as followed: β-actin (66,009–1–1 g, PROTEINTECH), Bclaf1 (26,809–1-AP, Santa Cruz Biotechnology), VPS35 (sc-374,372, Santa Cruz Biotechnology), HSF1 (sc-9144, Santa Cruz Biotechnology), Hsp70 (sc-69,705, Santa Cruz Biotechnology), Hsp90α (8165 s, Cell Signaling Technology), TSG101 (sc-7964, Santa Cruz Biotechnology), CD63 (25,682–1-AP, PROTEINTECH). The secondary antibodies (Donkey anti-mouse/rabbit IRDye 680/800) were purchased from Li-COR Biosciences (Lincoln, Nebraska, USA). Blots were scanned by LI-COR Odyssey infrared imaging system and quantified with Image J software v1.8.0.

Immunofluorescence microscopy

The treated cells were fixed in 4% paraformaldehyde for 15 min, washed with PBS, and permeabilized with precooled methanol at −20°C for 10 min. The immune detection was applied to cells incubated with anti-VPS35 (1:100, sc-374,372, Santa Cruz Biotechnology, USA), anti-Bclaf1 (1:100, 26,809–1-AP-150ul, PROTEINTECH, USA), anti-EEA1 (1:100, #3288, CST, USA), anti-GM130 (1:100, 12480S, CST, USA) overnight at 4°C. Then secondary antibodies Alexa Fluor 555 donkey anti-mouse IgG (1:200, A31570, ThermoFisher, USA) or Alexa Fluor 488 donkey anti-rabbit IgG (1:200, A21206, ThermoFisher, USA) were incubated in room temperature for 2 h in the dark. The nuclei were stained with DAPI for 5 min and images were taken with an Olympus FV1000 Confocal Laser Scanning Microscope (Olympus, Tokyo, Japan). The intensities and co-localization Ratio of both proteins were analyzed by Image Pro-plus 6.0.

Reverse transcription-PCR (RT-PCR)

Total RNA was isolated from Hepatoma cell lines using TRIZOL reagent (9109, Takara, Tokyo, Japan). 1 μg of purified RNA was used to reverse transcription into cDNA applying the Prime Script RT Reagent Kit (CRR047A, Takara, Tokyo, Japan) with gDNA Eraser. RT-PCR was performed using Premix Taq (R004A, Takara, Tokyo, Japan) with specific primers sequences. The cycling conditions were as followed: 1 cycle of 94°C for 5 min; 30 cycles of 94°C for 30 s, 55°C for 30 s, and 72°C for 20 s; 1 cycle of 72°C for 5 min, then cooled at 4°C for 10 min. The reaction was carried out on GeneAMP PCR System 9700 (Applied Biosystems, USA). Subsequently, electrophoresis was applied to separate the PCR products on an agarose gel and the relative mRNA levels were analyzed using Image J software v1.8.0. The sequence of primers was listed in Supplementary Table 1.

Chromatin immunoprecipitation and PCR (ChIP-PCR)

ChIP experiments were conducted according to the published protocol [30]. Briefly, DNA segments sonicated by Ultrasonic systems (Scientz JY88-II, China) were electrophoresed to separate on an agarose gel, which finally ranged from 100 to 500 bps. Bclaf1 interacted DNA fragments were precipitated by incubating the cell extract with 1 μg of Bclaf1-specific antibody (1:100, sc101388, Santa Cruz Biotechnology) overnight. The complexes were captured using Protein A/G-Sepharose beads (IP10–10ML, Millipore, MA, USA). The primers of VPS35-promoters were listed in Supplementary Table 1. The DNA samples were analyzed by RT-PCR and electrophoresis on a 2% agarose gel staining with Ethidium Bromide (EB).

Dual-Luciferase reporter assay

HepG2 cells were co-transfected with 1 μg luciferase reporter vector plasmid (pGL4.10 contains VPS35 promoter domain, KidanTM Biosciences, Guangzhou, China) and Bcalf1 full-length plasmid with Lipofectamine 3000 transfection reagent (L3000015, Life Technologies, USA) for 24–36 h, and Dual-Luciferase assay was then performed according to the manufactures' instructions of Dual-Luciferase Reporter Gene Assay Kit (Beyotime Biotechnology, Shanghai, China). The luminescence was detected by a Luminometer Microplate reader (TECAN Spark, Switzerland). Firefly luciferase was used as a reporter gene and renilla luciferase (pGL3-Renilla) as a normalized control.

Measurements of mitochondrial oxygen consumption rate [31]

To determine the effects of Control-EVs, STA9090-EVs and NB-EVs on mitochondrial function, we evaluated mitochondrial oxygen consumption rate in HepG2 cells via the Seahorse XFP Analyzer. In brief, 7000 cells were plated in Seahorse XFP 8 Cell Culture Mini-plates and co-cultured with 20 μg of C/STA9090/NB-EVs at 37 °C 5% CO_2 for 24 h. Subsequently, specific inhibitors of respiratory chain were used to be treated with cells at preset time points. The basal OCR values were measured at 2, 9 and 14 min. Then, OCR values were continued to measure at 21, 28 and 34 min after adding Oligomycin. And at 36 min, FCCP was added, and measures were taken at 41, 47, and 54 min. Ultimately, the OCR values were measured at 61, 67 and 74 min after Rotenone was added. The OCR values were normalized according to the cell density. The results of HepG2 cells treated with Control-EVs, STA9090-EVs and NB-EVs were calculated.

Nude mouse xenotransplantation experiments

Four-week-old BALB/C male nude (15–20 g) mice were obtained from the Laboratory Animal Center of Southern Medical University. 5×10^6 MHCC97H-RFP cells in 200μL basic DMEM were injected subcutaneously into both flanks of mice. After 10 days, mice were randomly divided into 3 groups according to the treatment, as follows: control group ($n = 5$), STA9090 group ($n = 5$) and NB group ($n = 5$). Hsp90 N terminal inhibitor STA9090 (dissolved in 10% DMSO, 18% Cremophor RH, 3.6% dextrose, 68.4% ddH$_2$O at 60°C, 25 mg/kg) and C terminal inhibitor NB (dissolved in DMSO, 50 mg/kg) were injected intraperitoneally into the mice of STA9090 group (25 mg/kg) or NB group (50 mg/kg) three times per week for 12 days. And the final solution without STA9090 and NB was injected intraperitoneally into mice of control groups. The weight of the mice and the longest and shortest diameters of the xenograft tumors were measured every two days. The volume was calculated as: (longest diameter*shortest diameter ^{2})/2. After 2 weeks, all mice were sacrificed and tumors were isolated, which were used for western blotting and immunohistochemistry. All experimental procedures were followed by the principle of randomized blind. And our study was approved by the IACUC (Institutional Animal Care and Use Committee) of Southern Medical University (Approval Code: L2020029).

Orthotopic liver tumor experiment

For orthotopic implantation, male BALB/c nude mice (5 weeks old, 18–20 g) were anesthetized with 4% (w/v) Chloral hydrate (ZS-C804539–100 g, Macklin, Shanghai, China) by intraperitoneal injection. Then, 1.5×10^6 shNC-GFP or shVPS35-GFP HepG2 cells in 100μL basic DMEM were surgically implanted into the left liver lobes of mice. Tumor growth was monitored by fluorescence with *in vivo* bioluminescence imaging system on day 7, and mice with similar tumor growth were randomly grouped for treatment: shNC—Control group ($n = 3$), shNC-STA9090 group ($n = 3$), shNC—NB group ($n = 3$), shVPS35-Control group ($n = 3$) and shVPS35-STA9090 group ($n = 3$). Hsp90 N terminal inhibitor STA9090 (dissolved in 10% DMSO, 18% Cremophor RH, 3.6% dextrose, 68.4% ddH$_2$O at 60°C, 25 mg/kg) and C terminal inhibitor NB (dissolved in DMSO, 50 mg/kg) were injected intraperitoneally into the mice of above groups at the dose of 25 mg/kg or 50 mg/kg three times per week for a total of five injections. The weight of mice was measured every two days. On day 12, all mice were imaged with *in vivo* fluorescence imaging system and executed, then, the livers were isolated and imaged with *in vivo* fluorescence imaging system again (Approval Code: L2020029).

Immunohistochemistry (IHC)

IHC was carried out on paraffin sections of fresh tumor tissues isolated from HCC patients and nude mice following the standard LSAB protocol (Dako, USA). The primary antibodies against VPS35 (1:300, sc-374,372, Santa Cruz Biotechnology) and Bclaf1 (1:100, sc-101,388, Santa Cruz Biotechnology) were used, and Isotype-matched IgG was used as negative controls. Quantitative analyses of IHC positive results were shown as brown staining which were analyzed by Image-Pro-Plus 6.0 to quantify as average optical density (AOD) [AOD=integrated optical density (IOD) SUM/ Area SUM].

Statistical analyses

All results were described as mean ± standard deviation (SD) from three independent experiments. Correlation was analyzed using Pearson correlation analysis. The *P* values were analyzed with two-tailed Student's t-tests or one-way ANOVA. All statistical analyses were performed by SPSS software v21.0 (IBM, USA), and the statistical significance was set at $P < 0.05$.
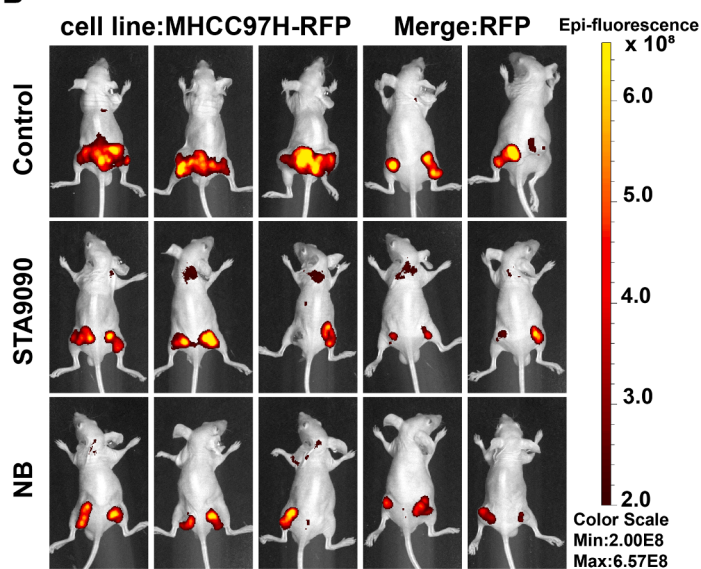
Result

N-terminal Hsp90 inhibitor STA9090 inhibits tumor growth but promotes invasion via STA9090-induced extracellular vesicles

Since Hsp90 inhibitor-related pro-metastatic effects were reported [19], to determine whether Hsp90 inhibitor STA9090 promotes metastasis, an orthotopic xenograft model of HCC was established by injecting HepG2-GFP cells into the left liver lobes of nude mice. Both STA9090 and NB could inhibit the growth of tumor as expected, however, more GFP signals spread out to different parts of livers in the mice treated with STA9090 compared with control group, but not in NB treated mice (Fig. 1A). To further clarify the pro-metastasis effect of STA9090, the subcutaneous xenografted tumors were transplanted in both flanks of nude mice with the cell line MHCC97H-RFP, which was stably transfected with red fluorescence protein (RFP) into the highly metastatic hepatocellular carcinoma cell MHCC97H. Then the mice were also treated with Hsp90 inhibitor STA9090 and NB. Consistently, more RFP signals spreading out to different parts of the animals were detected in STA9090 groups, while fewer RFP signals were detected in NB groups (Fig. 1B), though the volumes and weight of xenografted tumors decreased after STA9090 and NB treatment (Fig. 1C). Therefore, all these data supported that STA9090 treatment inhibited the growth of
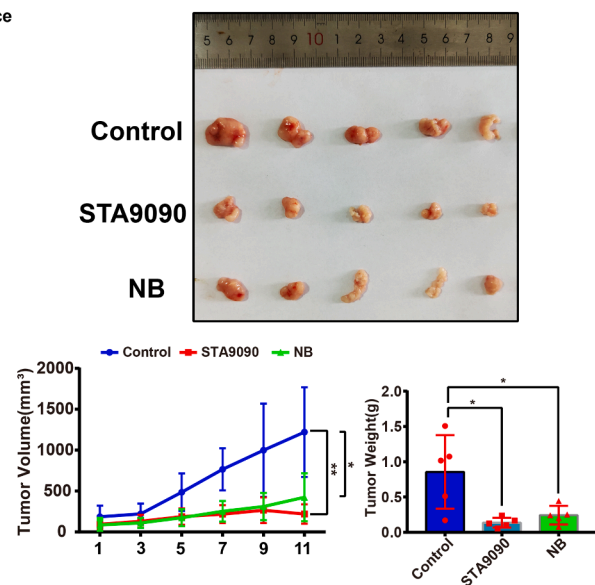
A
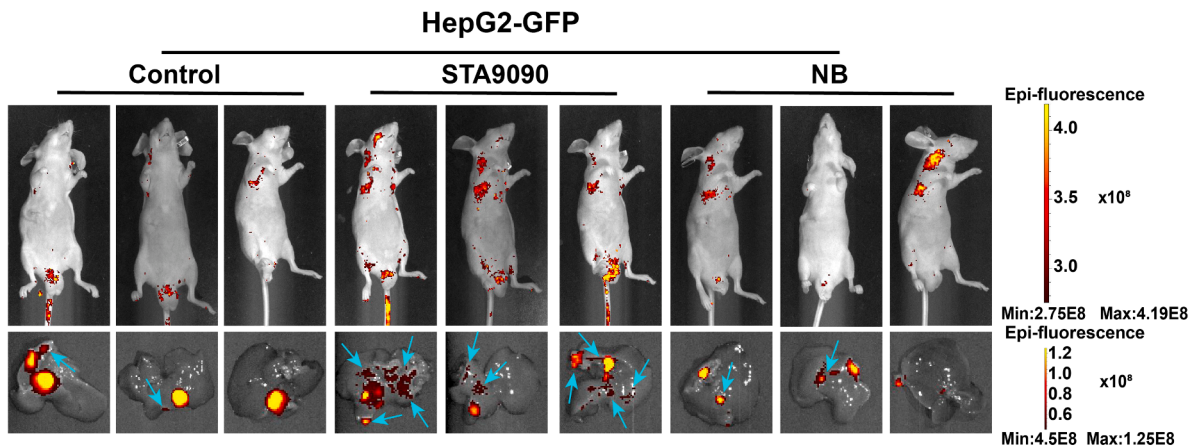
B

C

Fig. 1. N-terminal Hsp90 inhibitor STA9090 inhibits tumor growth but promotes invasion via STA9090-induced extracellular vesicles.
(A) HepG2-GFP cells (1.5×10^6) were used to establish an orthotopic liver cancer model. After 12 days, mice were randomly divided into control/STA9090/NB treated group. Fluorescence was evaluated by *in vivo* fluorescence image system. The appearance of representative mice tumors ($n = 3$) and liver cancer focus (blue arrow, $n = 3$) were shown. (B) MHCC97H-RFP cells (5×10^6 cells) were injected into both dorsal franks of 4–5 weeks old inbred BALB/c male nude mice to establish a xenograft tumor model. After 10 days, tumor-bearing mice (MHCC97H-RFP cells) were randomly divided into two groups as follows: Control ($n = 5$ mice), STA9090 ($n = 5$ mice) and NB ($n = 5$ mice). Mice with xenograft tumor were treated with STA9090 (25 mg/kg) and NB (50 mg/kg) for 12 days. Fluorescence of tumors after 12 days of STA9090 and NB treatment was evaluated by *in vivo* fluorescence imaging system; (C) growth curves and weight of xenograft tumors in mice treated with STA9090 and NB.

tumor but promoted metastasis.

To further characterize the overall difference in the protein components between Control-treated, STA9090-treated and NB-treated HepG2 cells, TMT (Tandem Mass Tag™) proteomics sequencing (LC-MS/MS) analysis was carried out. Interestingly, analysis of cellular components indicated that 87 proteins were associated with the "extracellular exosome" category in STA9090-treated cells, but not in NB-treated cells (Fig. S1). Hence, we next focused on the formation and role of EVs in the metastasis induced by Hsp90 NTD-binding inhibitor.

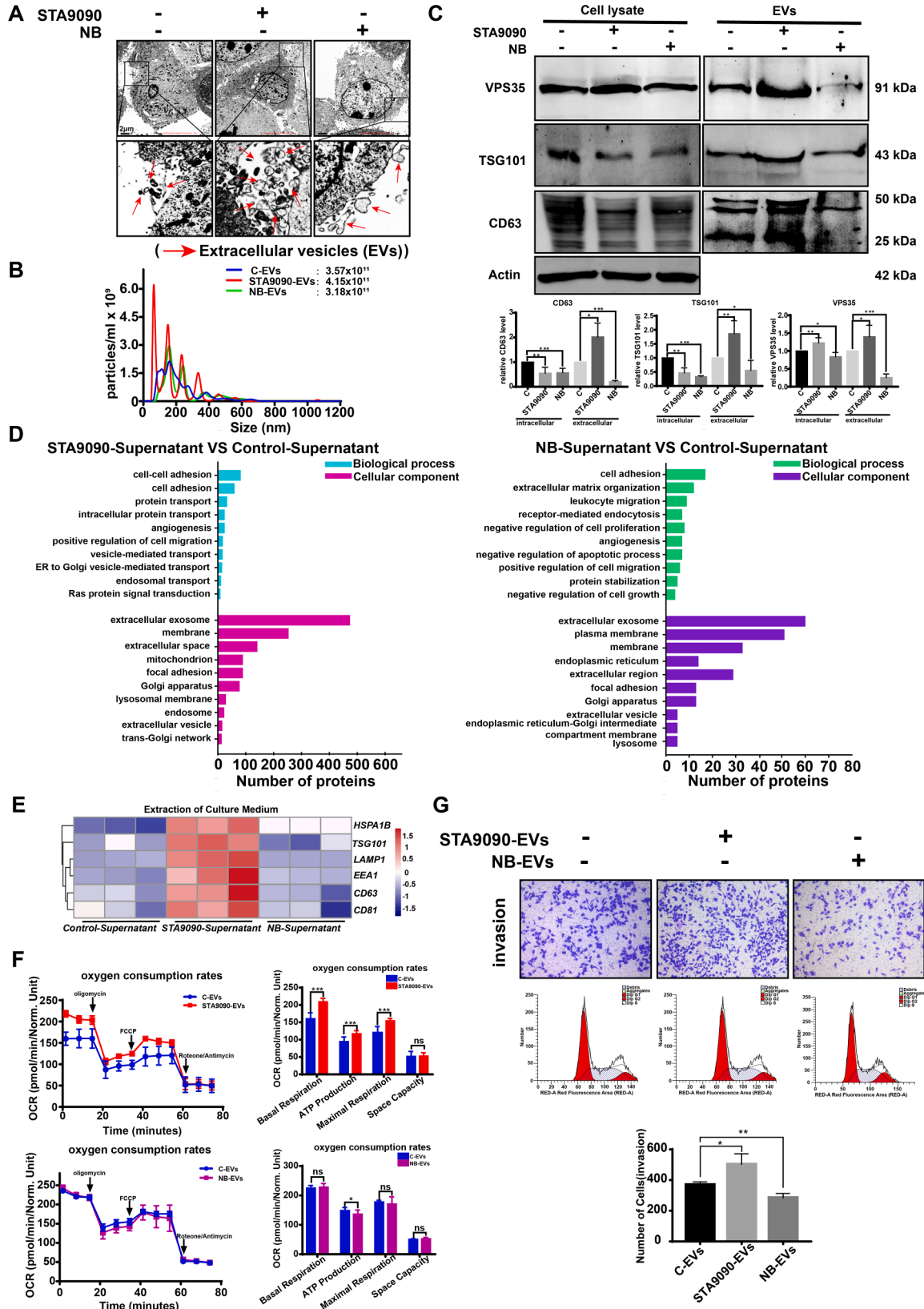*STA9090-induce EVs generation in HepG2 cells*

Experimental studies in mice suggested that chemotherapy has pro-metastatic effects with the release of extracellular vesicles (EVs) [7,32], and tumor cell-derived EVs, which promote the metastatic processes [33,34]. Whether STA9090 induced EVs played the pro-metastatic

effects were further explored. We isolated EVs from the culture medium of control, STA9090 and NB treated group, the extracellular vesicles extraction and purification procedure was shown in Fig. S2A. The size distribution of EVs was measured by Dynamic light scattering (DLS) (Fig. S2B), and the representative TEM images of EVs were further inspected by Transmission Electron Microscopy (TEM) (Fig. S2C, red arrows indicated).

The above data indicated that N terminal Hsp90 inhibitor STA9090 promoted HCC metastasis, thus we elicited a question: whether there is a componential difference between STA9090-induced-EVs and NB-induced-EVs? Interestingly, our TEM images showed that more EVs-like components could be observed in STA9090-treated cell surface, while larger EVs-like components could be observed in NB-treated cell surface (Fig. 2A, B, red arrows indicated). NTA analysis revealed a similar peak size of C-EVs, STA9090-EVs, and NB-EVs to that of EVs, and the total numbers of STA9090-EVs secreted was higher than C-EVs,

while the total numbers of NB-EVs was lower than C-EVs (Fig. 2B). In addition, to further determine the different effects of STA9090 and NB on EVs secretion and generation, CD63 and tumor susceptibility gene 101 (TSG101) which are the well-defined EVs markers [35] were

identified by western blotting, and the β-actin of cell lysate was used as a reference of cell numbers. As expected, the level of CD63, and TSG101 were significantly increased in the protein extract of the total EVs collected from culture medium of STA9090 treated cells, but decreased

(caption on next page)

Fig. 2. STA9090-induce EVs generation in HepG2 cells.
(A) HepG2 cell with STA9090 and NB treatments was analyzed by Transmission electron microscopy, arrowheads indicated the EVs (red arrows). (B) The size distribution traces and numbers of C/STA9090/NB-EVs were detected by NTA. The size of C-EVs is 215.4 ± 100.3, STA9090-EVs:191.4 ± 136.5, NB-EVs:244.3 ± 133.7; (C) The EVs-enriched and cell lysate protein fraction extracted from HepG2 cells with STA9090 and NB treatment were analyzed by immunoblotting for TSG101, CD63, and VPS35, the β-Actin of cell lysate was used as a reference of cell numbers. Value represent mean ± SD, $n = 3$ *$P < 0.01$, **$P < 0.01$, ***$P < 0.001$. (D) Enrichment analysis by biological process and cell component in proteins extracted from the culture medium of HepG2 cells treated with STA9090 and NB. (E) Hierarchical clustering of differentially expressed protein of EVs marker (Fold change >1.2 and Q value <0.05) between Control-Supernatant, STA9090-Supernatant, and NB-Supernatant, with protein abundance being Z-score normalized. Rows indicated proteins and columns indicated individual replicates. (F) The mitochondrial respiration of HepG2 cells treated with 20 μg of EVs purified from the culture medium of HepG2 cells with STA9090 and NB treatments was analyzed by Seahorse assay. Value represent mean ± SD, $n = 3$ *$P < 0.01$, **$P < 0.01$, ***$P < 0.001$. (G) Transwell invasion assay and cell cycle assay were performed with HepG2 cells treated with 2 μg of C-EVs, STA9090-EVs, and NB-EVs. Value represent mean ± SD, $n = 6$ *$P < 0.01$, **$P < 0.01$, ***$P < 0.001$. The scale is 200 μm.

in the protein extract of the total EVs collected from culture medium of NB treated cells. Increased VPS35 levels in cell lysate and EVs were also detected after STA9090 treatment, while both decreased after NB treatment (Fig. 2C). Therefore, we futher explored whether VPS35 was involved in the EVs formation and transport after STA9090 or NB treatment. The Gene Ontology (GO) enrichment analysis of differentially represented EVs proteins demonstrated that the enriched categories included vesicles-mediated transport in STA9090 supernatant. Furthermore, the mitochondrion component could be only found in STA9090 supernatant (Fig. 2D). TMT proteomics sequencing analysis of proteins extracted from culture medium showed that most of the EVs markers, like CD63, TSG101, Hsp70, EEA1, LAMP1, and CD81 were significantly increased in STA9090 supernatant (Fig. 2E), which is consistent with our western-blotting results. Our unpublished results indicated that increased VDAC1 in EVs might enhance the mitochondrial function of tumor cells which is vital for tumor metastasis. To determine whether C-EVs, STA9090-EVs, and NB-EVs could be absorbed by HepG2 cells, the C-EVs, STA9090-EVs, and NB-EVs were used in the EVs intake assays. As expected, the C-EVs, STA9090-EVs, and NB-EVs could be absorbed by HepG2 cells (Fig. S3). Thus, we further explored whether Hsp90 inhibitors-induced-EVs influenced the function of mitochondrial in more fundamental ways. A Seahorse mitochondrial function assay was performed on HepG2 cells treated with EVs isolating from the culture medium of control, STA9090, and NB group. We found that the basal respiration, mitochondrial ATP production, and maximal respiration were significantly increased in STA9090-EVs treated HepG2 cells compared to C-EVs, which indicated that STA9090-EVs could significantly increase the mitochondrial functionality of HepG2 cells, whereas NB-EVs did not affect the mitochondrial functionality of HepG2 cells (Fig. 2F). To further determine the potential of STA9090-EVs and NB-EVs on HepG2 cell invasion, the C-EVs, STA9090-EVs, and NB-EVs were used in the transwell invasion assays. As expected, STA9090-EVs facilitated the invasion of HepG2 cells, while NB-EVs inhibited the invasion of HepG2 cells, compared with control-EVs (Fig. 2G).

We also analyzed whether Hsp90 inhibitor STA9090 and NB affected the invasion of HepG2 cells using transwell invasion assay. We found that both STA9090 and NB induced G2 phase arrest and inhibited tumor invasion (Fig. S4). This result is consistent with the reduced tumor size after STA9090 treatment.

Collectively, these data showed that STA9090 induced the secretion of EVs, and the increased VPS35 after STA9090 treatment contributed to EVs release.

VPS35 is induced by STA9090 and promoted the EVs formation, delivery, secretion process and hcc invasion

Classically, vesicles with protein cargo could be sorted and packed in the Golgi apparatus, transported, and fused with plasma membrane (PM), which could be taken up by formation of early endosome (EE). In the early endosomes, proteins were either transported to PM or late endosome (LE) [36]. Several studies had demonstrated that early endosome protein marker EEA1 [12] was enriched in EE, while GM130 (Golgi apparatus marker) [37] was enriched in Golgi apparatus. VPS35 is important in regulating the retrieval and recycling of cargoes to

extracellular space by interacting with sorting receptors and delivering to trans-Golgi network (TGN) [36,38–40]. Therefore, we next explored how VPS35 was involved in the formation of EVs to exert its function. The immunofluorescence microscopy results demonstrated an increased co-localization of VPS35/GM130 (Fig. 3A), VPS35/EEA1 (Fig. 3B) after STA9090 treatment and a decreased co-localization after NB treatment. To investigate the relationship between VPS35 level and EVs secretion in STA9090-treated HepG2 cells, we down-regulated VPS35 expression in HepG2 cells by stably transfecting shVPS35 with lentivirus vectors. As shown in Fig. S5A, decreased VPS35 protein level after transfection was confirmed in cells companied with decreased Hsp70, CD63, and TSG101 levels in EVs (Fig. 3C). Moreover, immunofluorescence microscopy was used to determine the co-localization of VPS35-GM130 after siVPS35 in HepG2 cells. Consistent with our hypothesis, siVPS35 counteracted the STA9090-induced increase of the co-localization of VPS35-GM130. (Fig. 3D). We next determined the relevance of VPS35 levels and EVs released by STA9090-treated HepG2 cells for migration and invasion, siVPS35 could inhibit the migration and invasion of HepG2 cells (Fig. S5B, C). Next, HepG2 cells were supplied with EVs extracted from the culture medium of siNC, STA9090 plus siNC, siVPS35, and siVPS35 plus STA9090. Upon STA9090-induced EVs treatment, it induced a higher fraction of cells to invade to the lower chamber, but siVPS35 reduced the pro-invasion effect of STA9090-induced EVs (Fig. 3E left panel). In parallel, cell viability of HepG2 cells was determined to exclude the unspecific effect caused by differences in cell viability, revealing that the EVs treated with siNC, STA9090 plus siNC, siVPS35, and siVPS35 plus STA9090 had no effect on the viability of HepG2 cells, and the changes of invasion were caused by the level change of VPS35 (Fig. 3E right panel). Based on the shNC and shVPS35 cells treated with STA9090, the NTA analysis revealed that STA9090 could promote the EVs secretion and shVPS35 inhibited STA9090 induced EVs secretion (Fig. 3F). To further clarify the pro-metastasis effect of VPS35, an orthotopic xenograft model of HCC was established by injecting shNC-GFP (control HepG2 cells with GFP expression), and shVPS35-GFP (HepG2 cells with stably shVPS35 interfered) cells into the left liver lobes of nude mice. Comparing with the animals in shNC—C groups from the same batch of animal experiments shown in Fig. 1A, we found that the distant GFP signals in shVPS35-STA9090 group were reduced obviously comparing to shNC-STA9090 group and did not significantly increase compared with shVPS35-C group (Fig. 3G). Taken together, these data suggested that VPS35 mediated STA9090-induced EVs formation, delivery, and secretion to promote metastasis in HepG2 cells.

Upregulation of VPS35 levels positively correlates with Bclaf1 levels, poorer prognosis and higher metastasis in HCC

The above data revealed the different pro-metastatic effects caused by N-terminal Hsp90 inhibitor STA9090 and C-terminal Hsp90 inhibitor NB is VPS35 related. Since C-terminal Hsp90 inhibitor NB significantly decreased Bcl-2-associated transcription factor 1 (Bclaf1) protein level, which is a well-known transcription factor and one of the client proteins of Hsp90, we then focus on the relationship between Bclaf1 and VPS35. We analyzed the proteomics data [41] from the Chinese Human Proteome Projected (CNHPP) website (http://Liver.cnhpp.ncpsb.org/), and

the mRNA expression data from The Cancer Genome Atlas (TCGA; htt p://www.cancer.gov/). We found that both the protein (Fig. 4A) and mRNA (Fig. 4B) levels of VPS35 and Bclaf1 were upregulated in HCC. Moreover, there were a positive correlation between the protein and mRNA levels of Bclaf1 and VPS35 (Fig. 4C). Furthermore, subgroup analysis of multiple clinic pathological features of Liver Hepatocellular carcinoma in the TCGA (UALCAN: http://ualcan.path.uab.edu/index.

html) consistently showed high levels of VPS35, and Bclaf1. The Nodal metastasis status, cancer stages, and tumor grade boxplots of VPS35 and Bclaf1 gene were shown in Fig. 4D. The results demonstrated that the expression of the Bclaf1 and VPS35 genes were significantly associated with the metastasis of tumor. Moreover, higher VPS35 and Bclaf1 expression were associated with decreased overall survival in the 365 HCC patients (Fig. 4E). We next collected the tumor tissue and
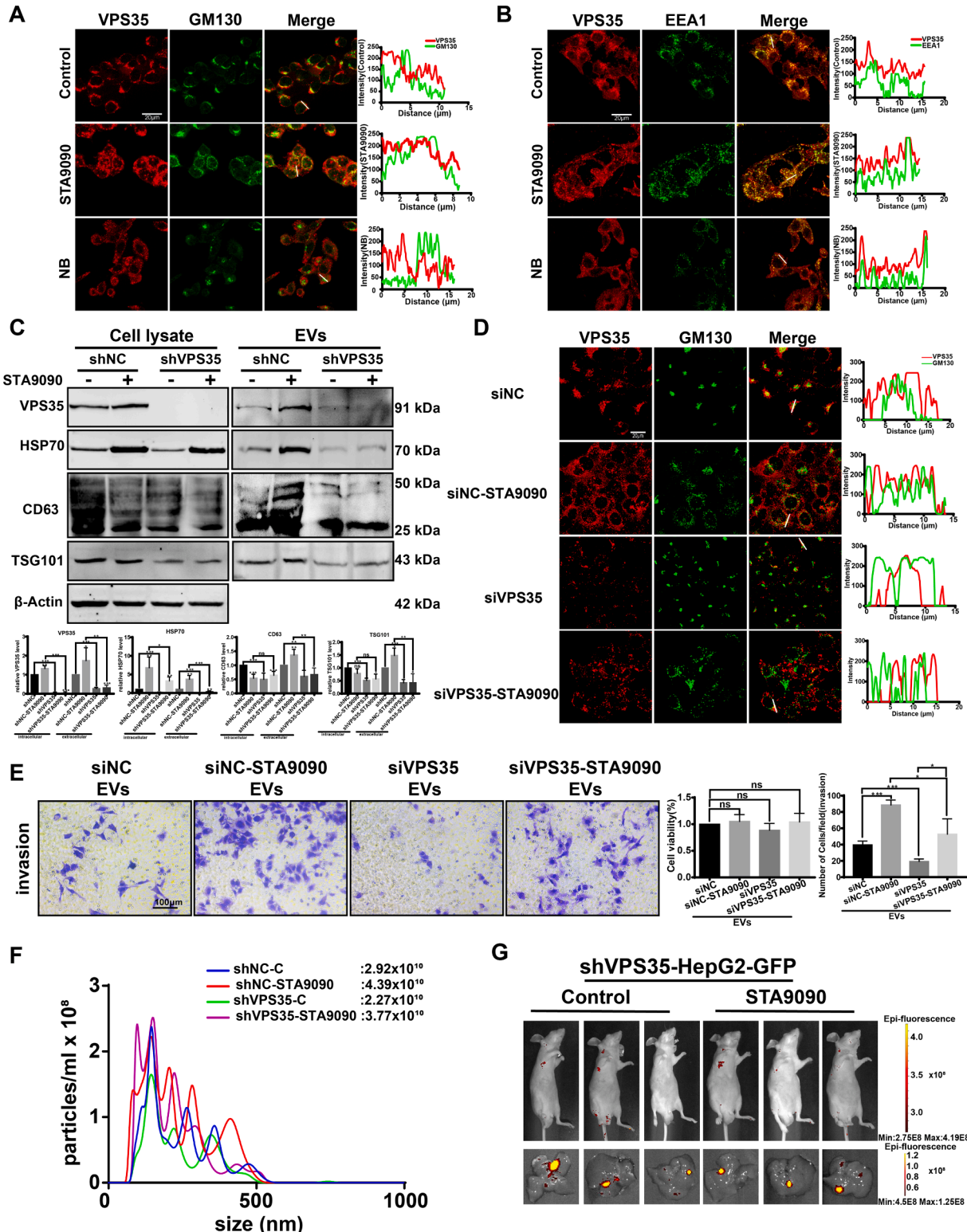
(caption on next page)

Fig. 3. VPS35 is induced by STA9090 and promoted the EVs formation, delivery, secretion process and HCC invasion.
(A) Confocal immunofluorescence images showed VPS35 (red) and GM130 (green) co-localization. Intensity plots of VPS35 and GM130 of the representative line of randomly selected cells for co-localization analysis. The Pearson's coefficient of VPS35 vs GM130 in control group is 0.516968, STA9090 group is 0.664415, NB group is 0.435422; (B) Confocal immunofluorescence images showed VPS35 (red) and EEA1 (green) co-localization. Intensity plots of VPS35 and EEA1 of the representative line of randomly selected cells for co-localization analysis. The Pearson's coefficient of VPS35 vs EEA1 in control group is 0.683207, STA9090 group is 0.781596, NB group is 0.648579; (C) The EVs and cell lysate protein, extracted from shNC/shVPS35 cell combined with STA9090 treatment, were analyzed by immunoblotting for TSG101, CD63, Hsp70, and VPS35, the β-Actin of cell lysate was used as a reference of cell numbers. Value represent mean ± SD, $n = 3$ *$P <$ 0.01, **$P <$0.01, ***$P<$ 0.001. (D) Confocal immunofluorescence images showed VPS35 (red) and GM130 (green) co-localization. Intensity plots of VPS35 and GM130 of the representative line of randomly selected cells for co-localization analysis. The Pearson's coefficient of VPS35 vs GM130 in siNC group is 0.415257, siNC-STA9090 group is 0.31523, siVPS35 group is 0.229758; siVPS35-STA9090 group is 0.092724; (E) Transwell invasion assays were performed with HepG2 cell incubated with EVs extracted from the conditioned medium of HepG2 cells treated with STA9090 in combination with siNC or siVPS35 sequence. Number of cells/ field were measured by Image Pro-plus6.0, and Value represent mean ± SD, $n = 6$ *$P < 0.01$, **$P <$0.01, ***$P < 0.001$. The scale is 100 μm. (F) The size distribution traces and numbers of shNC—C/shNC-STA9090/shVPS35-C/shVPS35-STA9090-EVs were detected by NTA. (G) shVPS35-GFP HepG2 cells (1.5×10^6) were used to establish an orthotopic liver cancer model. After 12 days, mice were randomly divided into shVPS35-C/shVPS35-STA9090 group. Fluorescence was evaluated by *in vivo* fluorescence image system. The appearance of representative mice tumors ($n = 3$) and livers ($n = 3$) were shown.

---

adjacent tissue samples from the livers of 11 HCC patients after operation, the expression of Bclaf1 and VPS35 was investigated using immunohistochemical (IHC) staining. The results showed the higher protein expression of Bclaf1 and VPS35 in tumor tissues compared with that in adjacent tissues (Fig. 4F). Furthermore, the protein and mRNA expression of VPS35 and Bclaf1 were also upregulated in liver cancer cell lines (Huh7, HepG2, and MHCC97H) when compared with the normal liver cell line L02 (Fig. S6A, B). These results indicated that upregulation of VPS35 levels positively correlates with Bclaf1 levels and poorer prognosis and higher metastasis in HCC.

N-terminal Hsp90 inhibitor STA9090 induced HSF1 activation and increased Bclaf1/VPS35 level in HCC

Based on the published study, Hsp90 N-terminal inhibitors trigger HSF1 activation, causing an increased transcription of HSP family members including Hsp27, Hsp70, and Hsp90, which is referred to as the heat shock response (HSR) and helps the survival of malignant cells [42]. As Bclaf1 is one of the Hsp90 client proteins, our previous data confirmed a positive correlation between the level of Bclaf1 and VPS35 in HCC. To further determined whether the NTD or CTD inhibitor of Hsp90 could activate HSF1, the protein levels of HSF1, Hsp90α, Hsp70, Bclaf1, and VPS35 were detected in HepG2 cells treated with STA9090 or NB. Consistently, STA9090 caused an increase of Hsp90α and Hsp70 protein levels which indicated STA9090 triggered HSF1 activation, whereas NB did not cause the obvious increase in Hsp90α and Hsp70 protein levels (Fig. 5A). Interestingly, STA9090 also induced an increased protein and mRNA levels of Bclaf1 and VPS35. However, NB induced the decreased protein and mRNA levels of Bclaf1 and VPS35 (Fig. 5A, B). These protein level changes were also supported by the immunofluorescence staining (Fig. 5C). The increased expression profile of Bclaf1 and VPS35 were detected in MHCC97H cells xenografted tumors from STA9090 group (Fig. S7A), while decreased levels of Bclaf1 and VPS35 were detected in HepG2-Luc cells xenografted tumors from NB group (Fig. S7B, C). Likewise, the expression of Bclaf1 and VPS35 in the tumor of Control, STA9090, and NB group was investigated using IHC staining. It showed a remarkably higher expression of Bcalf1 and VPS35 in STA9090-treated tumor compared to the Control-treated tumor, while a significantly lower expression in NB-treated tumor (Fig. 5D).

According to the above results, thus we wondered whether HSF1 also influenced Bcalf1 and VPS35 expression. To verify this, we found that the expression of Bclaf1, VPS35, Hsp90α, and Hsp70 proteins were significantly decreased in HepG2 cells transiently transfected with siHSF1 (Fig. S8). Collectively, these results suggested that HSF1 positively regulated Bclaf1 and VPS35 expression.

Bclaf1 upregulated VPS35 transcription through bZIP DNA binding domain in HCC cells

The above results indicated that the difference between STA9090 and NB was the expression of Bclaf1 and VPS35. And Bclaf1 was positively correlated with VPS35 in HCC patients. In addition, we found that there was a transcription binding site of Bclaf1 in the VPS35 promoter region by interrogating the data from the public database of Genecards (https://www.genecards.org/) and Cistrome data Browser (http://cistrome.org/db/#/). Thus, we wondered whether Bclaf1 regulates VPS35 transcription. To check this possibility, we designed a set of primers that spanned the sequence from −140 to −233 bps of the VPS35 promoter (Fig. 6A, upper panel). The ChIP assay in HepG2 cells was carried out to determine the effect of STA9090 treatment on the recruitment of Bclaf1 to the promoter of VPS35. The results revealed that VPS35 promoter could be pulled down by anti-Bclaf1 antibodies and confirmed that STA9090 dramatically increased the binding of Bclaf1 to VPS35 promoter (Fig. 6A, lower panel). Therefore, we speculated that Bclaf1, as a transcriptional factor, participated in the process of VPS35 transcription. We next examined the effects of the siBclaf1 or the Bclaf1-FL plasmid on the expression of VPS35. We found that the protein and mRNA levels of VPS35 decreased in HepG2 and Huh7 cells transiently transfected with siBclaf1, while increased in cells transfected with Bclaf1-FL plasmid (Fig. 6B, C). These data indicated that Bclaf1 upregulated the transcription of VPS35. Besides, the ChIP assay was further to carried out to verify whether the protein level of Bclaf1 affected the binding to the promoter region of VPS35 gene. The results revealed that knocked down Bcalf1 expression in HepG2 cells significantly decreased the binding of Bcalf1 on VPS35 promoter (Fig. 6D, left panel), while Bclaf1 overexpression in HepG2 cells remarkably increased the binding of Bclaf1 on VPS35 promoter (Fig. 6D, middle panel). Additionally, the VPS35 promoter was inserted in front of the firefly luciferase reporter gene to detect the effect of Bclaf1 on VPS35 transcription. Consistently, the luciferase activity (Luciferase/Renilla) was also obviously decreased when HepG2 cells were transfected with siBclaf1 but increased when transfected with the Bclaf1 overexpression plasmid (Fig. 6D right panel). Collectively, these results supported that N-terminal Hsp90 inhibitor STA9090 increased the binding of Bclaf1 on VPS35 promoter and Bclaf1 positively regulated VPS35 transcription in HCC.

Bclaf1 protein has a basic zipper (bZIP) domain and a Myb homologous DNA-binding domain, both bind to DNA and function as a transcriptional regulator [27]. To further illustrate which domain of Bclaf1 was necessary for VPS35 transcription, we prepared expression plasmids encoding Flag-tagged constructs of different domains of Bclaf1, containing the sequences for full-length Bclaf1 (FL), a Myb domain deleted variant(△Myb), a bZIP domain deleted variant (△bZIP), and the empty vector (EV) as control (Fig. 6E upper panel). A series of Flag-tagged Bclaf1 plasmids were transiently transfected into HepG2 cells and verified by western blot (Fig. 6E lower panel). To identify whether Myb and bZIP domains were involved in the regulation of Bclaf1 with VPS35,
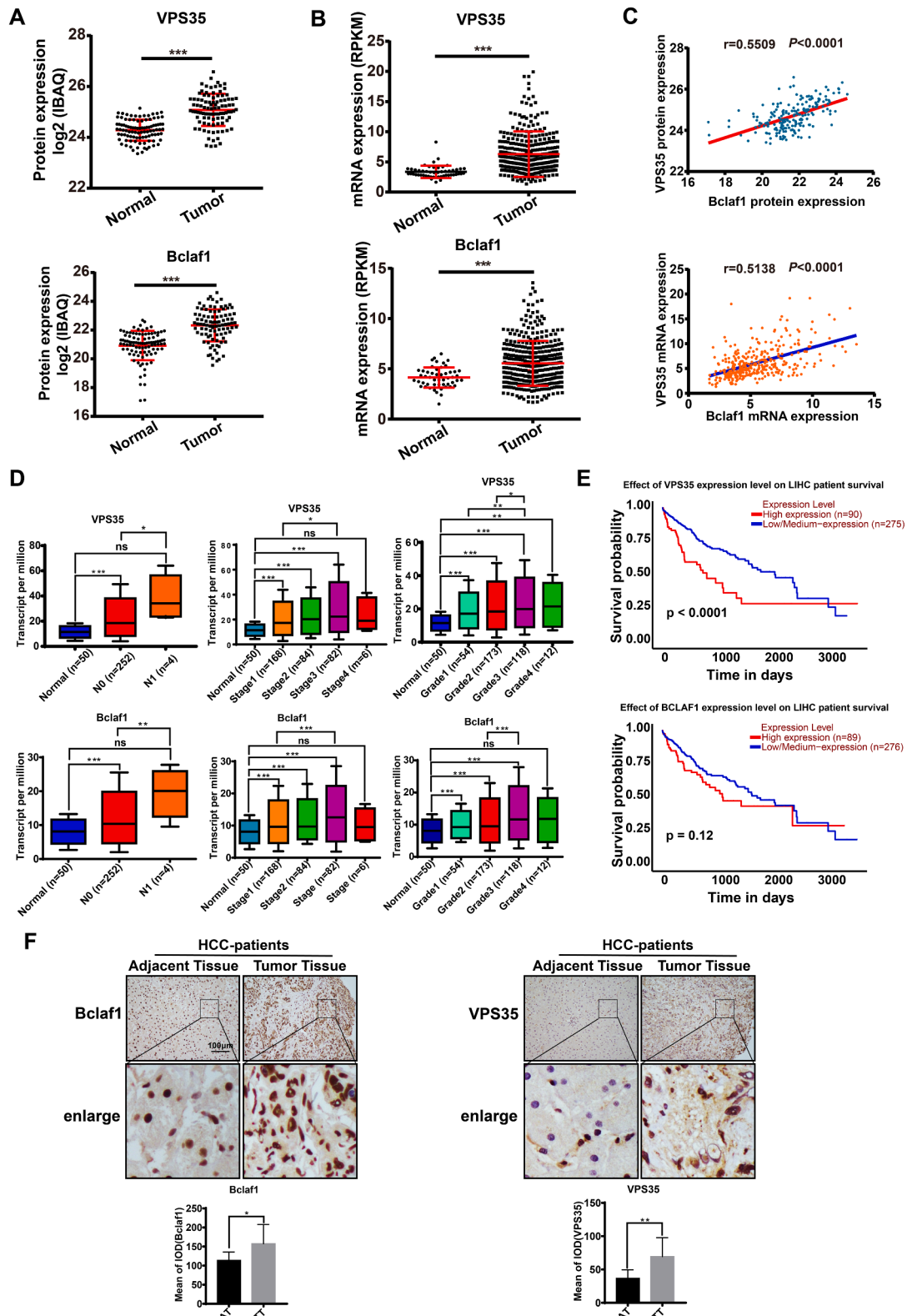
Fig. 4. Upregulation of VPS35 levels positively correlates with Bclaf1 levels, poorer prognosis and higher metastasis in HCC.
We analyzed data obtained from the CNHPP data portal. Increased protein (A) and mRNA (B) levels of VPS35 and Bclaf1 of patients with HCC. (C) A positive correlation between the protein ($r = 0.5509$, $P<0.0001$) and mRNA ($r = 0.5138$, $P<0.0001$) levels of Bclaf1 and VPS35. (D) Relative expression of Bclaf1 and VPS35 genes in normal tissues and liver hepatocellular carcinoma tissues with different nodal metastasis status, cancer stage, and tumor grade. (E) UALCAN survival analysis of patients with HCC based on VPS35 and Bclaf1 protein level. (F) The protein expression of Bclaf1 and VPS35 in tumor tissue (TT) or adjacent tissue (AT) of patients with HCC was detected by IHC.
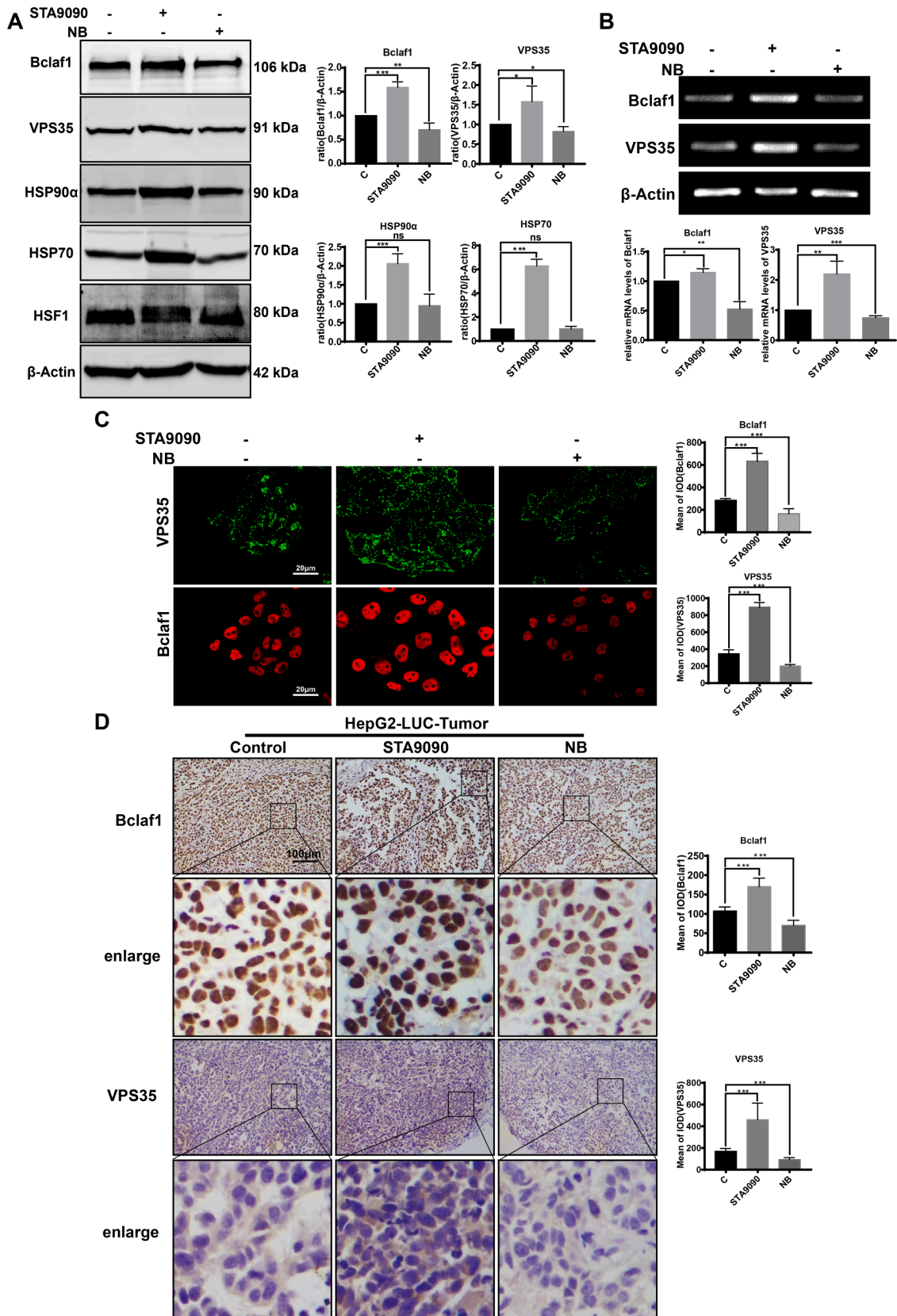
Fig. 5. N-terminal Hsp90 inhibitor STA9090 induced HSF1 activation and increased Bclaf1/VPS35 level in HCC.
(A) HepG2 cells were incubated with 0.1μmol/L STA9090 and 0.5 mmol/L NB for 24 h as indicated. Protein levels of Bclaf1, VPS35, Hsp90α, Hsp70, and HSF1 were determined by western blotting and (B) mRNA levels of Bclaf1 and VPS35 were determined by RT-PCR analysis. (C)Confocal immunofluorescence images showed VPS35 (red) and Bclaf1 (green) intensity. (D) Protein levels of Bclaf1 and VPS35 in Control, STA9090, and NB-treated tumors were detected by immunohisto-chemistry. Image Pro-plus 6.0 software was used to quantify the Mean of IOD and Value represent mean ± SD, $n = 6$ *$P < 0.01$, **$P < 0.01$, ***$P < 0.001$.
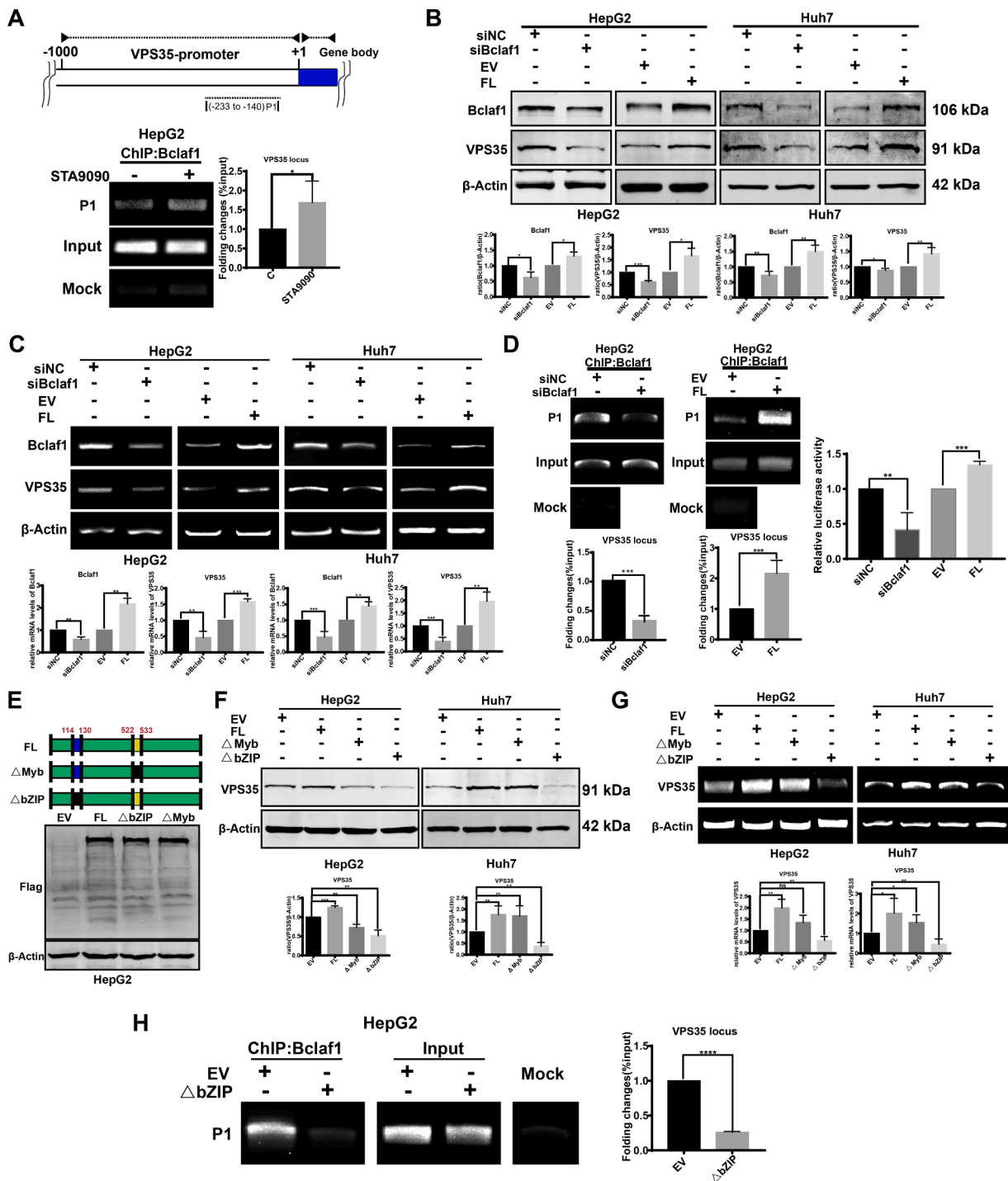
Fig. 6. Bclaf1 upregulated VPS35 transcription through bZIP DNA binding domain in HCC cells.
(A) The schematic representation of VPS35 promoter with the indicated region (P1) for PCR analysis. HepG2 cell was incubated with STA9090 for 24 h. ChIP-PCR was adopted to measure Bclaf1 binding on VPS35 promoter region. (B, C) HepG2 and Huh7 cells were transiently transfected with siNC, siBclaf1, EV plasmid, and FL plasmid. The Bclaf1 and VPS35 level were measured by western blotting and RT-PCR. (D) HepG2 cells were transfected with siNC and siBclaf1 for 48 h or transfected with EV and FL plasmids for 24 h. ChIP-PCR was adopted to measure Bclaf1 binding on VPS35 promoter region. And HepG2 cells were co-transfected with VPS35 promoter-luciferase reporter plasmids and siNC or siBclaf1 or EV plasmid or FL plasmid. Luciferase reporter gene assay was carried out to detect the interaction between Bclaf1 and VPS35 promoter region. The luciferase activity decreased transiently transfected with siBclaf1 and increased transiently transfected with Bclaf1-FL plasmid. (E) Schematic structure of Bclaf1 domains (upper panel). HepG2 cells were transfected with different Bclaf1-encoding plasmids for 24 h and the transfection efficiency was confirmed by western blot (lower panel). (F, G) HepG2 cells were transiently transfected with EV, FL, ΔMyb, and ΔbZIP plasmids for 24 h. The VPS35 protein and mRNA levels were measured by western blot and RT-PCR. (H) HepG2 cells were transiently transfected with EV and ΔbZIP plasmids for 24 h. ChIP-PCR was adopted to measure Bclaf1 binding on VPS35 promoter region. Image J software v1.8.0 was used to quantify the bands relative intensities and Value represent mean ± SD, $n = 3$ *$P < 0.01$, **$P < 0.01$, ***$P < 0.001$.

HepG2 and Huh7 cells were transfected with different Bclaf1 mutants. The protein and mRNA levels of VPS35 were dramatically decreased when transiently transfected with △bZIP plasmid in HepG2 and Huh7 cells, compared to the EV vector (Fig. 6F, G). The ChIP assay was subsequently performed to further confirm whether the Bclaf1-mediated regulation of VPS35 transcription is correlated with the basic zipper (bZIP) homologous DNA-binding motif. HepG2 cells were transiently transfected with △bZIP plasmid and the empty vector (EV), and the results showed that the binding of Bclaf1 on VPS35 promoter was significantly reduced after transfecting with △bZIP plasmid (Fig. 6H). Therefore, these results demonstrated that the bZIP domain was necessary for the binding of Bclaf1 on VPS35 promoter and bZIP domain of Bclaf1 positively regulated VPS35 transcription.

N-terminal Hsp90 inhibitor STA9090 promotes HCC metastasis via Bclaf1-VPS35-EVs axis in HCC

The above results demonstrated that Bclaf1 positively regulated the transcription of VPS35. Thus, we elicited a hypothesis on whether STA9090 promotes HCC metastasis via Bclaf1-VPS35-EVs axis. Hence, we designed a series of experiments to confirm this hypothesis. Firstly, knockdown of Bclaf1 by transfecting with siRNA targeting Bclaf1 suppressed the VPS35 expression in HepG2 cells compared to the siNC-treatment. Consistently, the level of VPS35 decreased after treatment with STA9090 in combination with siBclaf1, compared with the treatment of siNC plus STA9090 (Fig. 7A). Then, siVPS35 couldn't decrease the expression of Bclaf1 compared to the siNC, and the level of Bclaf1 was still increased after treatment with siVPS35 in combination with STA9090 (Fig. 7B), revealing that STA9090 increased VPS35 level via Bclaf1. To further confirm the regulation of Bclaf1 on VPS35, HepG2 cells were transiently transfected with siVPS35 and Bclaf1-FL plasmid. The results showed that siVPS35 caused the decreased level of VPS35 could be rescued by the overexpression of Bclaf1 compared with siNC treatment (Fig. 7C). Our previous results proved that Bclaf1 facilitated the angiogenesis and proliferation in HCC under hypoxia. Next, to elucidate whether Bclaf1 is vitally involved in HCC metastasis, we
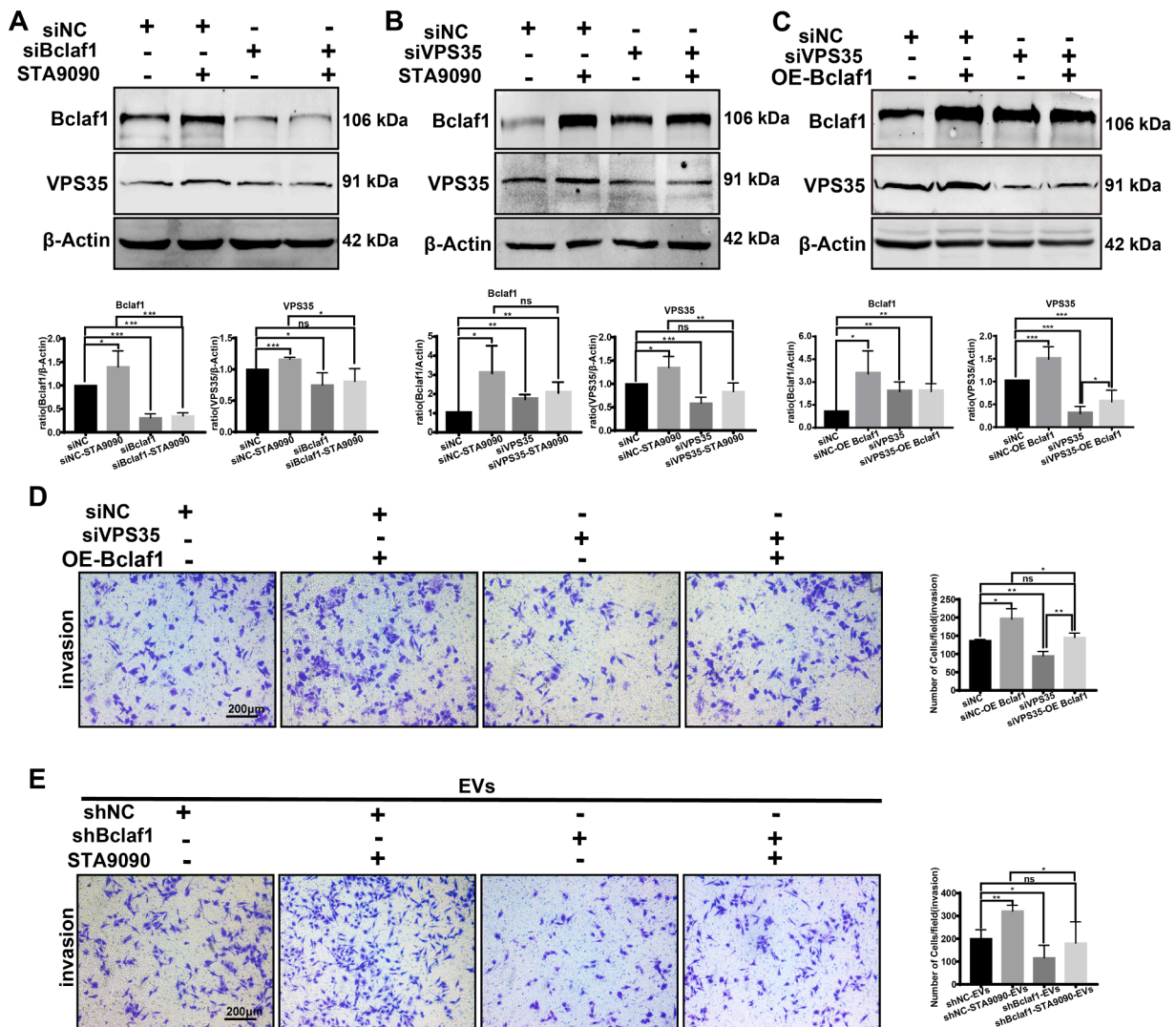

Fig. 7. N-terminal Hsp90 inhibitor STA9090 promotes HCC metastasis via Bclaf1-VPS35-EVs axis in HCC.
(A, B) HepG2 cells treated with NC-siRNA, NC-siRNA plus STA9090, Bclaf1-siRNA, and Bclaf1-siRNA plus STA9090 or treated with NC-siRNA, NC-siRNA plus STA9090, VPS35-siRNA, and VPS35-siRNA plus STA9090 for 48 h. The Bclaf1 and VPS35 levels were detected using western blotting. (C) HepG2 cells were transiently co-transfected with siVPS35 and Bclaf1-FL plasmid for 48 h. The Bclaf1 and VPS35 levels were detected using western blotting. Image J software v1.8.0 was used to quantify the bands relative intensities and Value represent mean ± SD, $n = 3$ *$P < 0.01$, **$P < 0.01$, ***$P < 0.001$. (D) Transwell invasion assays were performed with HepG2 cells transfected either with siNC, siNC-Bclaf1-FL plasmid, siVPS35, and siVPS35-Bclaf1-FL plasmid. (E) Transwell invasion assays were performed with HepG2 cell incubated with 2 µg of EVs extracted from the culture medium of shNC/shBclaf1 stable lentivirus cell lines either treated with STA9090. Number of cells/field were measured by Image Pro-plus6.0, and Value represent mean ± SD, $n = 6$ *$P < 0.01$, **$P < 0.01$, ***$P < 0.001$. The scale is 200 µm.

evaluated the migratory and invasive capacity of Bclaf1 by Transwell assay. We found that the migration and invasion were significantly decreased in HepG2 cells transfecting with siRNA targeting Bclaf1. In addition, cells transiently transfected with Bclaf1 overexpression plasmid could rescue the siBclaf1-treated decrease of migration and invasion (Fig. S9A). We also presumed whether bZIP domain affected the HepG2 cells invasion. The cells transfected with △bZIP plasmid induced a fewer fraction of cells to invade to the lower chamber (Fig. S9B). To further investigate whether VPS35 participated in the HCC metastasis. As it showed in Fig. 7D, the invasion of HepG2 cells co-transfected with siVPS35 and Bclaf1-FL plasmid was partially decreased compared to co-transfected with siNC and Bclaf1-FL plasmid. Taken together, our data strongly supported the causal role of VPS35 involving in the HCC metastasis, and Bclaf1 facilitated the HCC metastasis via the positive regulation of VPS35. To further explore whether Bcalf1 contributed to the increased invasion capability caused by STA9090-induced EVs, we found that EVs extracted from STA9090-treated cells caused more cells invading to the lower chamber, but shBcalf1 counteracted the invasion-promoting effects of STA9090-EVs (Fig. 7E). Collectively, all these data suggested that N-terminal Hsp90 inhibitor STA9090 promotes HCC metastasis via Bclaf1-VPS35-EVs axis in HCC.

Discussion

In this study, we obtained important insights into Hsp90 inhibitor on VPS35 transcription regulation mechanism and VPS35 related EVs formation. NTD binding Hsp90 inhibitor STA9090 treatment activated HSF1, increased the levels of Bclaf1 and promoted the transcription of VPS35 via its bZIP DNA binding domain by directly binding to the VPS35 promoter, consequently leading to the increase of VPS35 protein. Upregulated VPS35 protein promoted the EVs delivery process from Golgi-apparatus, early endosome, late endosome (or Multiple vesicles body), and eventually secreted to extracellular space to exert its function in HCC metastasis (Fig. 8). These *in vitro* data explained why the expression of Bclaf1 and VPS35 positively correlate with each other and correlated with metastasis in the xenograft tumor animal model.

Molecular chaperone protein is required for cells to maintain the folding, stability, and activation of intracellular proteins [18]. Interestingly, Hsp90 is commonly increased in malignant tumors, and preclinical studies showed that Hsp90 inhibitors were effective against the growth of tumor, angiogenesis, and metastasis in the xenograft nude mice model. In sight of this, Hsp90 inhibitor has been considered a promising anti-tumor drug for clinical use in humans, especially for cancer therapy [43,44]. However, none of the clinical trials of Hsp90 inhibitors monotherapy have been approved by FDA to date. A few cases of occurrence of bone metastasis [19, 45] were reported in animal
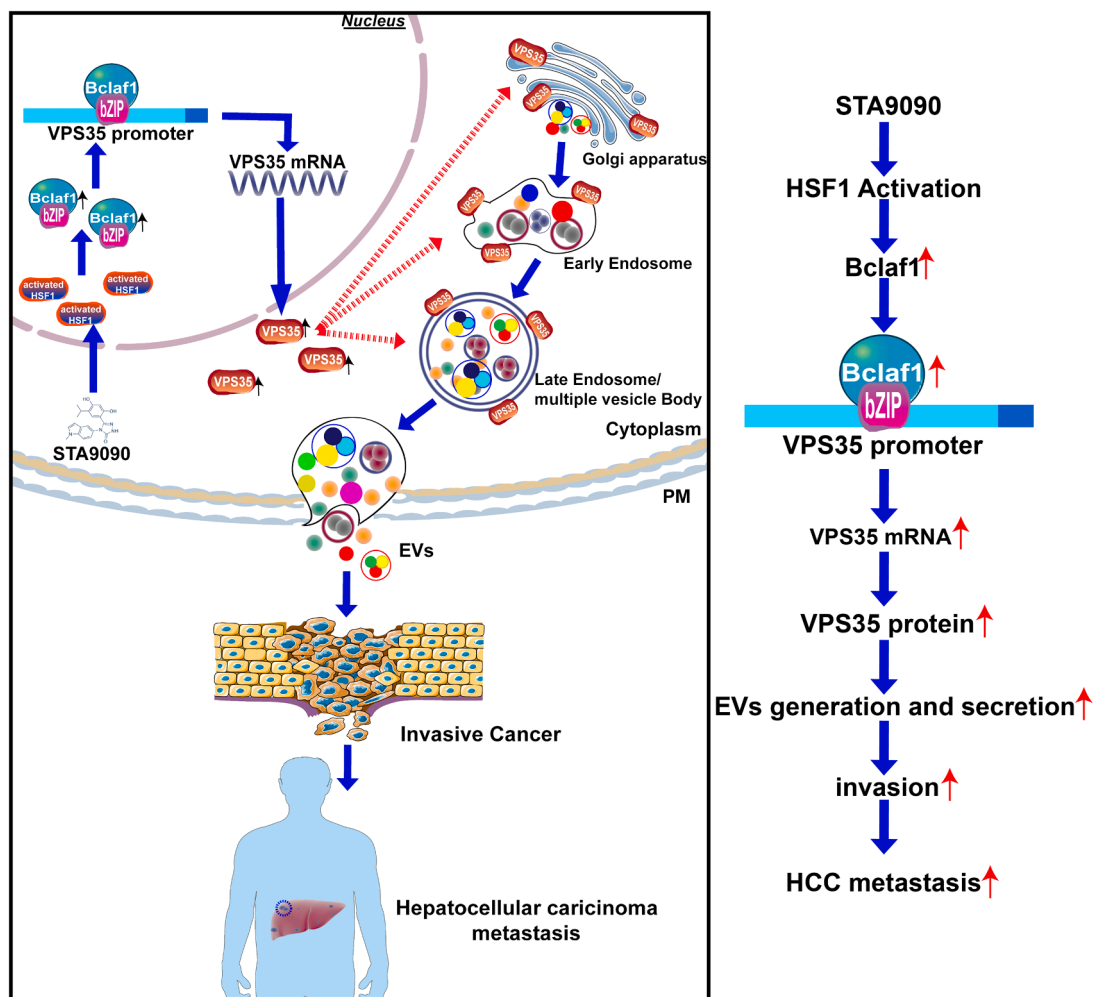

Fig. 8. Model for the HSF1-Bclaf1-VPS35-EVs connection in HCC.
STA9090 treatment activated HSF1 and increased levels of Bclaf1, which promoted the transcription of VPS35 by directly binding to the VPS35 promoter via its bZIP DNA binding domain, consequently leading to the increase of VPS35 protein. Upregulated VPS35 protein promoted the EVs delivery process from Golgi-apparatus, early endosome, late endosome (or Multiple vesicles body), and eventually secreted to extracellular space to exert its function in HCC metastasis.

models treated with Hsp90 N-terminal inhibitors, without deep investigation on its molecular mechanism. Our study now linked NTD Hsp90 inhibitors to HSF1-Bclaf1-VPS35 axis and metastasis in HCC.

VPS35 had been reported in Parkinson disease patients, which is vital for regulating the retrieval and recycling of cargoes to TGN or plasma membrane, or other organelles [9], but the role of retromer in neuronal EV traffic [46] is still unclear. Interestingly, VPS35, as a novel potential oncogene in LIHC, can exerts its oncogenic roles to promote tumor growth, invasion and metastasis through the PI3K/AKT signaling pathway [13]. However, the detailed mechanism of VPS35 affecting the progress of HCC is still unknown. A recent review reported that various type of cargo is taken up by cell endocytosis and the EVs sorted, packed, and secreted from Golgi apparatus are transported to the early endosome, which is either recycled to the PM or sequestered into the ILV of MVBs, subsequently formated into late endosome or multiple vesicular bodies and secreted to the extracellular space [47]. Likewise, our findings demonstrated that VPS35 is necessary for exporting EVs from Golgi apparatus or early endosome to late endosome (multiple vesicles bodies) and eventually to extracellular space (Fig. 3). Except for the transportive function of EVs, VPS35 is reported to be involved in transcriptional regulation, since it had been verified that the mRNA level of DLP1 was increased in VPS35-overexpressing cells [48]. Our results also demonstrated the increased VPS35 levels in cell lysate (Fig. 2C), together with 87 proteins were associated with the "extracellular exosome" category in STA9090-treated cells (Fig. S1). Consistently, a decrease in EVs biomarkers (TSG101, CD63, and Hsp70) was observed in shVPS35 cells. Taken together, this finding suggested that VPS35 affected both the expression of EVs related proteins and inhibit the secretion of EVs.

It is well-known that EVs are required for tumor microenvironmental communication, like metastatic process, and metabolism of cancers [49–51]. Chemotherapy is widely used as an effective cancer therapy. However, experimental studies in mice suggest that chemotherapy has pro-metastatic effects with the release of extracellular vesicles (EVs), which facilitate the seeding and growth of metastatic cancer cells in distant organs [7,32]. Though recent evidence suggests that chemotherapeutic drugs can promote metastasis, the underneath mechanisms are poorly defined, especially how chemotherapy drives tumor derived EVs release remains unclear. Consistently, we found that knockdown of the expression of VPS35 could decrease the EVs secretion and inhibit HCC metastasis. While STA9090 could increase the EVs secretion and promote HCC metastasis. And our seahorse assay indicated a key role for STA9090-induced EVs in mitochondrial basal respiration, ATP production, and Maximal respiration. These findings suggested that STA9090-EVs could be absorbed by HepG2 cells (Fig. S3), which would enhance the invasive ability of HepG2 cells. Interestingly, downregulating the expression of VPS35 combined with STA9090 treatment would decrease the metastasis compared with monotherapy of STA9090. So the above results indicate that VPS35 mediated STA9090-induced EVs formation, transport, and secretion to promote metastasis in HepG2 cells.

The active HSF1 plays an important part in cellular response causing the expression of Heat shock proteins, which can protect cells from damage [52]. HSF1 expression and activity were always increased in tumors and involved in carcinogenesis [53]. Several studies reported that knockdown of HSF1 strongly inhibited the proliferation and reduced the migration and invasion of tumor cells [54–56]. Other studies showed that HSF1 could promote invasion and metastasis of hepatocellular carcinoma via Hsp27 [57]. And it showed that HSF1 activity was correlated with metastasis in a large cohort of breast cancer patients [58]. Our results showed that HSF1, as an important transcription factor, could be activated by NTD binding Hsp90 inhibitor, leading to activating the transcription of genes like Hsp27, Hsp70, and Hsp90. Bclaf1 was originally considered to be a pro-apoptosis factor and it can cause cell cycle arrest [25, 59]. However, recent studies assigned that Bclaf1 functioned as an oncogene in some human tumors. We had verified that Bclaf1 regulated HIF-1α transcription via binding to the

promoter of HIF-1α gene and facilitated the angiogenesis of HCC during hypoxia. One of the main differences between NTD and CTD binding Hsp90 inhibitors was the expression of Bclaf1 and VPS35 and HSF1 activation (Fig. 5). Interestingly, the protein and mRNA levels VPS35 and Bclaf1 were increased or decreased under STA9090 or NB treatment respectively (Fig. 5). It suggested that HSF1 could regulate the expression of Bclaf1 and VPS35 (Fig. S7), but the detailed mechanism still needs to be further explored.

The migration and invasion of HepG2 cells were decreased or increased under transfected with siBclaf1 or Bclaf1-FL plasmid (Fig. S9A). Online data mining revealed that VPS35 and Bclaf1 expression were significantly increased in HCC patients and Bclaf1 was positively correlated with VPS35 (Fig. 4), these results suggested that Bclaf1 supports metastasis by driving transcription of VPS35. Till now, the only reported transcription factor for VPS35 is KLF7, which might enhance the transcription of VPS35 [15]. However, the Cistromic (ChIP-seq) regulation report from SPP (The Signaling Pathways Project) for VPS35 (https://www.signalingpathways.org/) revealed that there are hundreds of transcription factors binding on VPS35 promoter region under physiological status (Table 1), including a group transcription factors with bZIP DNA binding domain.

The bZIP transcription factors, as the DNA-binding proteins, were involved in the gene expression programs, such as cell proliferation, and apoptosis [60,61]. The bZIP TFs contain a dimerization domain and a DNA-binding domain [62], which make direct contact with specific DNA sequences and stabilize DNA-protein interactions [63]. The cellular bZIP TFs motif exists in the AP-1 complexes (Jun, Fos, ATF, and Maf families), C/EBP complexes, and CREB complexes [62]. As for the induction of HIF1A transcription, bZIP DNA binding domain was essential [26]. Here, we demonstrated that Bclaf1 was directly bound to the VPS35 promoter via its bZIP DNA-binding domain (Fig. 6H), and STA9090 could increase Bclaf1 binding to the VPS35 promoter and upregulate VPS35 transcription (Fig. 6A).

We identified that the Bcalf1-VPS35 axis facilitated HCC-metastasis, and further confirmed that Bclaf1 functioned as an upstream regulator of VPS35. In addition, we found that knockdown of the expression of Bclaf1 could decrease the VPS35 level, and ultimately inhibited the EVs secretion, leading to a decrease in VPS35 level in EVs and suppressing the tumor invasion. Taken together, our study confirmed that Hsp90 inhibitor STA9090-induced EVs promoted invasion and metastasis by HSF1-Bclaf1-VPS35-EVs axis in hepatocellular carcinoma, which might provide novel combination therapeutic targets and strategies to reduce the metastasis of HCC or other solid tumors, and provide a feasible idea to counteract the EVs related metastasis induced by other traditional chemotherapeutic treatment.

Authors' contributions

Wenchong Tan: Resources, Data curation, Software, Formal analysis, Validation, Investigation, methodology, writing-original draft, writing-review and editing

Jinxin Zhang: investigation, data curation, software, methodology, validation

Lixia Liu: methodology, writing-original draft, writing-review and editing

Manfeng Liang: data curation, validation

Jieyou Li: investigation

Zihao Deng, Zhenming Zheng: data curation

Yaotang Deng: software

Yan Li, Guantai Xie: data curation

Jiajie Zhang: Instrument support

Fei Zou: Conceptualization, funding acquisition, validation

Xuemei Chen: Conceptualization, funding acquisition, supervision, investigation, methodology, writing-original draft, writing-review and editing;

Declaration of Competing Interest

None.

Acknowledgments

Supplementary materials

Supplementary material associated with this article can be found, in the online version, at doi:10.1016/j.tranon.2022.101502.

References

[1] H. Takayama, M. Ohta, Y. Iwashita, H. Uchida, Y. Shitomi, K. Yada, M. Inomata, Altered glycosylation associated with dedifferentiation of hepatocellular carcinoma: a lectin microarray-based study, BMC Cancer 20 (2020) 192.

[2] H. Sung, J. Ferlay, R.L. Siegel, M. Laversanne, I. Soerjomataram, A. Jemal, F. Bray, Global Cancer Statistics 2020: GLOBOCAN Estimates of Incidence and Mortality Worldwide for 36 Cancers in 185 Countries, CA Cancer J. Clin. 71 (2021) 209–249.

[3] S. Du, X. Song, Y. Li, Y. Cao, F. Chu, O.A. Durojaye, Z. Su, X. Shi, J. Wang, J. Cheng, T. Wang, X. Gao, Y. Chen, W. Zeng, F. Wang, D. Wang, X. Liu, X. Ding, Celastrol inhibits ezrin-mediated migration of hepatocellular carcinoma cells, Sci. Rep. 10 (2020) 11273.

[4] D.I. Cantor, H.R. Cheruku, J. Westacott, J.S. Shin, A. Mohamedali, S.B. Ahn, Proteomic investigations into resistance in colorectal cancer, Expert Rev. Proteom. 17 (2020) 49–65.

[5] J.J. Lin, A.T. Shaw, Resisting Resistance: targeted Therapies in Lung Cancer, Trends Cancer 2 (2016) 350–364.

[6] S. Atay, S. Banskota, J. Crow, G. Sethi, L. Rink, A.K. Godwin, Oncogenic KIT-containing exosomes increase gastrointestinal stromal tumor cell invasion, Proc. Natl. Acad. Sci. U S A, 111 (2014) 711–716.

[7] I. Keklikoglou, C. Cianciaruso, E. Guc, M.L. Squadrito, L.M. Spring, S. Tazzyman, L. Lambein, A. Poissonnier, G.B. Ferraro, C. Baer, A. Cassara, A. Guichard, M. L. Iruela-Arispe, C.E. Lewis, L.M. Coussens, A. Bardia, R.K. Jain, J.W. Pollard, M. De Palma, Chemotherapy elicits pro-metastatic extracellular vesicles in breast cancer models, Nat. Cell Biol. 21 (2019) 190–202.

[8] F. Xiao, H. Li, Z. Feng, L. Huang, L. Kong, M. Li, D. Wang, F. Liu, Z. Zhu, Y. Wei, W. Zhang, Intermedin facilitates hepatocellular carcinoma cell survival and invasion via ERK1/2-EGR1/DDIT3 signaling cascade, Sci. Rep. 11 (2021) 488.

[9] K.J. McMillan, H.C. Korswagen, P.J. Cullen, The emerging role of retromer in neuroprotection, Curr. Opin. Cell Biol. 47 (2017) 72–82.

[10] M. Seaman, The Retromer Complex: from Genesis to Revelations, Trends Biochem. Sci 46 (2021) 608–620.

[11] R.W. Choy, M. Park, P. Temkin, B.E. Herring, A. Marley, R.A. Nicoll, M. von Zastrow, Retromer mediates a discrete route of local membrane delivery to dendrites, Neuron 82 (2014) 55–62.

[12] J. Follett, A. Bugarcic, Z. Yang, N. Ariotti, S.J. Norwood, B.M. Collins, R.G. Parton, R.D. Teasdale, Parkinson disease-linked Vps35 R524W mutation impairs the endosomal association of retromer and induces alpha-synuclein aggregation, J. Biol. Chem. 291 (2016) 18283–18298.

[13] G. Zhang, X. Tang, L. Liang, W. Zhang, D. Li, X. Li, D. Zhao, Y. Zheng, Y. Chen, B. Hao, K. Wang, N. Tang, K. Ding, DNA and RNA sequencing identified a novel oncogene VPS35 in liver hepatocellular carcinoma, Oncogene 39 (2020) 3229–3244.

[14] Y. Liu, H. Deng, L. Liang, G. Zhang, J. Xia, K. Ding, N. Tang, K. Wang, Depletion of VPS35 attenuates metastasis of hepatocellular carcinoma by restraining the Wnt/PCP signaling pathway, Genes Dis. 8 (2021) 232–240.

[15] Y. Guo, B. Chai, J. Jia, M. Yang, Y. Li, R. Zhang, S. Wang, J. Xu, KLF7/VPS35 axis contributes to hepatocellular carcinoma progression through CCDC85C-activated beta-catenin pathway, Cell Biosci. 11 (2021) 73.

[16] Y. Wu, Y. Ding, X. Zheng, K. Liao, The molecular chaperone Hsp90 maintains Golgi organization and vesicular trafficking by regulating microtubule stability, J. Mol. Cell Biol. 12 (2020) 448–461.

[17] J.T. Price, J.M. Quinn, N.A. Sims, J. Vieusseux, K. Waldeck, S.E. Docherty, D. Myers, A. Nakamura, M.C. Waltham, M.T. Gillespie, E.W. Thompson, The heat shock protein 90 inhibitor, 17-allylamino-17-demethoxygeldanamycin, enhances osteoclast formation and potentiates bone metastasis of a human breast cancer cell line, Cancer Res. 65 (2005) 4929–4938.

[18] J. Sanchez, T.R. Carter, M.S. Cohen, B. Blagg, Old and new approaches to target the Hsp90 chaperone, Curr. Cancer Drug Targets 20 (2020) 253–270.

[19] S. Takeuchi, K. Fukuda, S. Arai, S. Nanjo, K. Kita, T. Yamada, E. Hara, H. Nishihara, H. Uehara, S. Yano, Organ-specific efficacy of HSP90 inhibitor in multiple-organ

[20] metastasis model of chemorefractory small cell lung cancer, Int. J. Cancer 138 (2016) 1281–1289.

[20] S. Chaudhury, B.M. Keegan, B. Blagg, The role and therapeutic potential of Hsp90, Hsp70, and smaller heat shock proteins in peripheral and central neuropathies, Med. Res. Rev. 41 (2021) 202–222.

[21] S. Santagata, R. Hu, N.U. Lin, M.L. Mendillo, L.C. Collins, S.E. Hankinson, S. J. Schnitt, L. Whitesell, R.M. Tamimi, S. Lindquist, T.A. Ince, High levels of nuclear heat-shock factor 1 (HSF1) are associated with poor prognosis in breast cancer, Proc. Natl. Acad. Sci. U. S. A. 108 (2011) 18378–18383.

[22] Y. Liao, Y. Xue, L. Zhang, X. Feng, W. Liu, G. Zhang, Higher heat shock factor 1 expression in tumor stroma predicts poor prognosis in esophageal squamous cell carcinoma patients, J. Transl. Med. 13 (2015) 338.

[23] M.L. Mendillo, S. Santagata, M. Koeva, G.W. Bell, R. Hu, R.M. Tamimi, E. Fraenkel, T.A. Ince, L. Whitesell, S. Lindquist, HSF1 drives a transcriptional program distinct from heat shock to support highly malignant human cancers, Cell 150 (2012) 549–562.

[24] X. Zhou, Y. Wen, Y. Tian, M. He, X. Ke, Z. Huang, Y. He, L. Liu, A. Scharf, M. Lu, G. Zhang, Y. Deng, Y. Yan, M.P. Mayer, X. Chen, F. Zou, Heat shock protein 90alpha-dependent B-cell-2-associated transcription factor 1 promotes hepatocellular carcinoma proliferation by regulating MYC proto-oncogene c-MYC mRNA stability, Hepatology 69 (2019) 1564–1581.

[25] G.M. Kasof, L. Goyal, E. White, Btf, a novel death-promoting transcriptional repressor that interacts with Bcl-2-related proteins, Mol. Cell. Biol. 19 (1999) 4390–4404.

[26] Y. Wen, X. Zhou, M. Lu, M. He, Y. Tian, L. Liu, M. Wang, W. Tan, Y. Deng, X. Yang, M.P. Mayer, F. Zou, X. Chen, Bclaf1 promotes angiogenesis by regulating HIF-1alpha transcription in hepatocellular carcinoma, Oncogene 38 (2019) 1845–1859.

[27] A.W. Shao, H. Sun, Y. Geng, Q. Peng, P. Wang, J. Chen, T. Xiong, R. Cao, J. Tang, Bclaf1 is an important NF-kappaB signaling transducer and C/EBPbeta regulator in DNA damage-induced senescence, Cell Death Differ. 23 (2016) 865–875.

[28] G.V. Shelke, C. Lasser, Y.S. Gho, J. Lotvall, Importance of exosome depletion protocols to eliminate functional and RNA-containing extracellular vesicles from fetal bovine serum, J. Extracell. Vesicles 3 (2014).

[29] M.A. Rider, S.N. Hurwitz, D.J. Meckes, ExtraPEG: a polyethylene glycol-based method for enrichment of extracellular vesicles, Sci. Rep. 6 (2016) 23978.

[30] J.D. Nelson, O. Denisenko, P. Sova, K. Bomsztyk, Fast chromatin immunoprecipitation assay, Nucleic Acids Res. 34 (2006) e2.

[31] V. Singh, M.I. Khalil, A. De Benedetti, The TLK1/Nek1 axis contributes to mitochondrial integrity and apoptosis prevention via phosphorylation of VDAC1, Cell Cycle 19 (2020) 363–375.

[32] C.A. Wills, X. Liu, L. Chen, Y. Zhao, C.M. Dower, J. Sundstrom, H.G. Wang, Chemotherapy-induced upregulation of small extracellular vesicle-associated PTX3 accelerates breast cancer metastasis, Cancer Res. 81 (2021) 452–463.

[33] X. Mao, S.K. Tey, C. Yeung, E. Kwong, Y. Fung, C. Chung, L.Y. Mak, D. Wong, M. F. Yuen, J. Ho, H. Pang, M.P. Wong, C.O. Leung, T. Lee, V. Ma, W.C. Cho, P. Cao, X. Xu, Y. Gao, J. Yam, Nidogen 1-enriched extracellular vesicles facilitate extrahepatic metastasis of liver cancer by activating pulmonary fibroblasts to secrete tumor necrosis factor receptor 1, Adv. Sci. (Weinh) 7 (2020), 2002157.

[34] X. Mao, L. Zhou, S.K. Tey, A. Ma, C. Yeung, T.H. Ng, S. Wong, B. Liu, Y. Fung, E. J. Patz, P. Cao, Y. Gao, J. Yam, Tumour extracellular vesicle-derived Complement Factor H promotes tumorigenesis and metastasis by inhibiting complement-dependent cytotoxicity of tumour cells, J. Extracell. Vesicles 10 (2020) e12031.

[35] A. Becker, B.K. Thakur, J.M. Weiss, H.S. Kim, H. Peinado, D. Lyden, Extracellular vesicles in cancer: cell-to-cell mediators of metastasis, Cancer Cell 30 (2016) 836–848.

[36] H. Kalra, G.P. Drummen, S. Mathivanan, Focus on extracellular vesicles: introducing the next small big thing, Int. J. Mol. Sci. 17 (2016) 170.

[37] X. Li, Y. Xia, S. Huang, F. Liu, Y. Ying, Q. Xu, X. Liu, G. Jin, C.J. Papasian, J. Chen, M. Fu, X. Huang, Identification of the interaction of VP1 with GM130 which may implicate in the pathogenesis of CVB3-induced acute pancreatitis, Sci. Rep. 5 (2015) 13324.

[38] L. Moran, F.J. Cubero, Extracellular vesicles in liver disease and beyond, World J. Gastroenterol. 24 (2018) 4519–4526.

[39] M. Malloci, L. Perdomo, M. Veerasamy, R. Andriantsitohaina, G. Simard, M. C. Martinez, Extracellular vesicles: mechanisms in human health and disease, Antioxid. Redox. Signal. 30 (2019) 813–856.

[40] E.T. Williams, X. Chen, D.J. Moore, VPS35, the Retromer Complex and Parkinson's Disease, J. Parkinsons Dis. 7 (2017) 219–233.

[41] Y. Jiang, A. Sun, Y. Zhao, W. Ying, H. Sun, X. Yang, B. Xing, W. Sun, L. Ren, B. Hu, C. Li, L. Zhang, G. Qin, M. Zhang, N. Chen, M. Zhang, Y. Huang, J. Zhou, Y. Zhao, M. Liu, X. Zhu, Y. Qiu, Y. Sun, C. Huang, M. Yan, M. Wang, W. Liu, F. Tian, H. Xu, J. Zhou, Z. Wu, T. Shi, W. Zhu, J. Qin, L. Xie, J. Fan, X. Qian, F. He, Proteomics identifies new therapeutic targets of early-stage hepatocellular carcinoma, Nature 567 (2019) 257–261.

[42] J.M. Park, Y.J. Kim, S. Park, M. Park, L. Farrand, C.T. Nguyen, J. Ann, G. Nam, H. J. Park, J. Lee, J.Y. Kim, J.H. Seo, A novel HSP90 inhibitor targeting the C-terminal domain attenuates trastuzumab resistance in HER2-positive breast cancer, Mol. Cancer 19 (2020) 161.

[43] S.A. Eccles, A. Massey, F.I. Raynaud, S.Y. Sharp, G. Box, M. Valenti, L. Patterson, B. A. de Haven, S. Gowan, F. Boxall, W. Aherne, M. Rowlands, A. Hayes, V. Martins, F. Urban, K. Boxall, C. Prodromou, L. Pearl, K. James, T.P. Matthews, K.M. Cheung, A. Kalusa, K. Jones, E. McDonald, X. Barril, P.A. Brough, J.E. Cansfield, B. Dymock, M.J. Drysdale, H. Finch, R. Howes, R.E. Hubbard, A. Surgenor, P. Webb, M. Wood, L. Wright, P. Workman, NVP-AUY922: a novel heat shock protein 90 inhibitor active against xenograft tumor growth, angiogenesis, and metastasis, Cancer Res. 68 (2008) 2850–2860.

[44] M.R. Jensen, J. Schoepfer, T. Radimerski, A. Massey, C.T. Guy, J. Brueggen, C. Quadt, A. Buckler, R. Cozens, M.J. Drysdale, C. Garcia-Echeverria, P. Chene, NVP-AUY922: a small molecule HSP90 inhibitor with potent antitumor activity in preclinical breast cancer models, Breast Cancer Res. 10 (2008) R33.

[45] K. Vermeulen, E. Naus, M. Ahamed, B. Attili, M. Siemons, K. Luyten, S. Celen, J. Schymkowitz, F. Rousseau, G. Bormans, Evaluation of [(11)C]NMS-E973 as a PET tracer for *in vivo* visualisation of HSP90, Theranostics 9 (2019) 554–572.

[46] R.B. Walsh, E.C. Dresselhaus, A.N. Becalska, M.J. Zunitch, C.R. Blanchette, A. L. Scalera, T. Lemos, S.M. Lee, J. Apiki, S. Wang, B. Isaac, A. Yeh, K. Koles, A. A. Rodal, Opposing functions for retromer and Rab11 in extracellular vesicle traffic at presynaptic terminals, J. Cell Biol. 220 (2021).

[47] E. Braschi, V. Goyon, R. Zunino, A. Mohanty, L. Xu, H.M. McBride, Vps35 mediates vesicle transport between the mitochondria and peroxisomes, Curr. Biol. 20 (2010) 1310–1315.

[48] W. Wang, X. Wang, H. Fujioka, C. Hoppel, A.L. Whone, M.A. Caldwell, P.J. Cullen, J. Liu, X. Zhu, Parkinson's disease-associated mutant VPS35 causes mitochondrial dysfunction by recycling DLP1 complexes, Nat. Med. 22 (2016) 54–63.

[49] H. Peinado, M. Aleckovic, S. Lavotshkin, I. Matei, B. Costa-Silva, G. Moreno-Bueno, M. Hergueta-Redondo, C. Williams, G. Garcia-Santos, C. Ghajar, A. Nitadori-Hoshino, C. Hoffman, K. Badal, B.A. Garcia, M.K. Callahan, J. Yuan, V.R. Martins, J. Skog, R.N. Kaplan, M.S. Brady, J.D. Wolchok, P.B. Chapman, Y. Kang, J. Bromberg, D. Lyden, Melanoma exosomes educate bone marrow progenitor cells toward a pro-metastatic phenotype through MET, Nat. Med. 18 (2012) 883–891.

[50] D.G. Phinney, M. Di Giuseppe, J. Njah, E. Sala, S. Shiva, C.C. St, D.B. Stolz, S. C. Watkins, Y.P. Di, G.D. Leikauf, J. Kolls, D.W. Riches, G. Deiuliis, N. Kaminski, S. V. Boregowda, D.H. McKenna, L.A. Ortiz, Mesenchymal stem cells use extracellular vesicles to outsource mitophagy and shuttle microRNAs, Nat. Commun. 6 (2015) 8472.

[51] A. O'Loghlen, Role for extracellular vesicles in the tumour microenvironment, Philos. Trans. R. Soc. Lond. B Biol. Sci. 373 (2018).

[52] P.K. Sorger, Heat shock factor and the heat shock response, Cell 65 (1991) 363–366.

[53] Y. Wang, J.R. Theriault, H. He, J. Gong, S.K. Calderwood, Expression of a dominant negative heat shock factor-1 construct inhibits aneuploidy in prostate carcinoma cells, J. Biol. Chem. 279 (2004) 32651–32659.

[54] Y. Nakamura, M. Fujimoto, S. Fukushima, A. Nakamura, N. Hayashida, R. Takii, E. Takaki, A. Nakai, M. Muto, Heat shock factor 1 is required for migration and invasion of human melanoma *in vitro* and *in vivo*, Cancer Lett. 354 (2014) 329–335.

[55] Y.D. Yao, T.M. Sun, S.Y. Huang, S. Dou, L. Lin, J.N. Chen, J.B. Ruan, C.Q. Mao, F. Y. Yu, M.S. Zeng, J.Y. Zang, Q. Liu, F.X. Su, P. Zhang, J. Lieberman, J. Wang, E. Song, Targeted delivery of PLK1-siRNA by ScFv suppresses Her2+ breast cancer growth and metastasis, Sci. Transl. Med. 4 (2012) 130ra48.

[56] S.A. Kim, S.M. Kwon, J.H. Yoon, S.G. Ahn, The antitumor effect of PLK1 and HSF1 double knockdown on human oral carcinoma cells, Int. J. Oncol. 36 (2010) 867–872.

[57] F. Fang, R. Chang, L. Yang, Heat shock factor 1 promotes invasion and metastasis of hepatocellular carcinoma *in vitro* and *in vivo*, Cancer Am. Cancer Soc. 118 (2012) 1782–1794.

[58] R.L. Carpenter, S. Sirkisoon, D. Zhu, T. Rimkus, A. Harrison, A. Anderson, I. Paw, S. Qasem, F. Xing, Y. Liu, M. Chan, L. Metheny-Barlow, B.C. Pasche, W. Debinski, K. Watabe, H.W. Lo, Combined inhibition of AKT and HSF1 suppresses breast cancer stem cells and tumor growth, Oncotarget 8 (2017) 73947–73963.

[59] J.P. McPherson, H. Sarras, B. Lemmers, L. Tamblyn, E. Migon, E. Matysiak-Zablocki, A. Hakem, S.A. Azami, R. Cardoso, J. Fish, O. Sanchez, M. Post, R. Hakem, Essential role for Bclaf1 in lung development and immune system function, Cell Death Differ. 16 (2009) 331–339.

[60] E. Shaulian, M. Karin, AP-1 as a regulator of cell life and death, Nat. Cell Biol. 4 (2002) E131–E136.

[61] C. Nerlov, The C/EBP family of transcription factors: a paradigm for interaction between gene expression and proliferation control, Trends Cell Biol. 17 (2007) 318–324.

[62] M.L. Stolz, C. McCormick, The bZIP Proteins of Oncogenic Viruses, Viruses 12 (2020).

[63] C. Vinson, M. Myakishev, A. Acharya, A.A. Mir, J.R. Moll, M. Bonovich, Classification of human B-ZIP proteins based on dimerization properties, Mol. Cell. Biol. 22 (2002) 6321–6335.